HRS

A HIGH RIGIDITY SPECTROMETER FOR FRIB

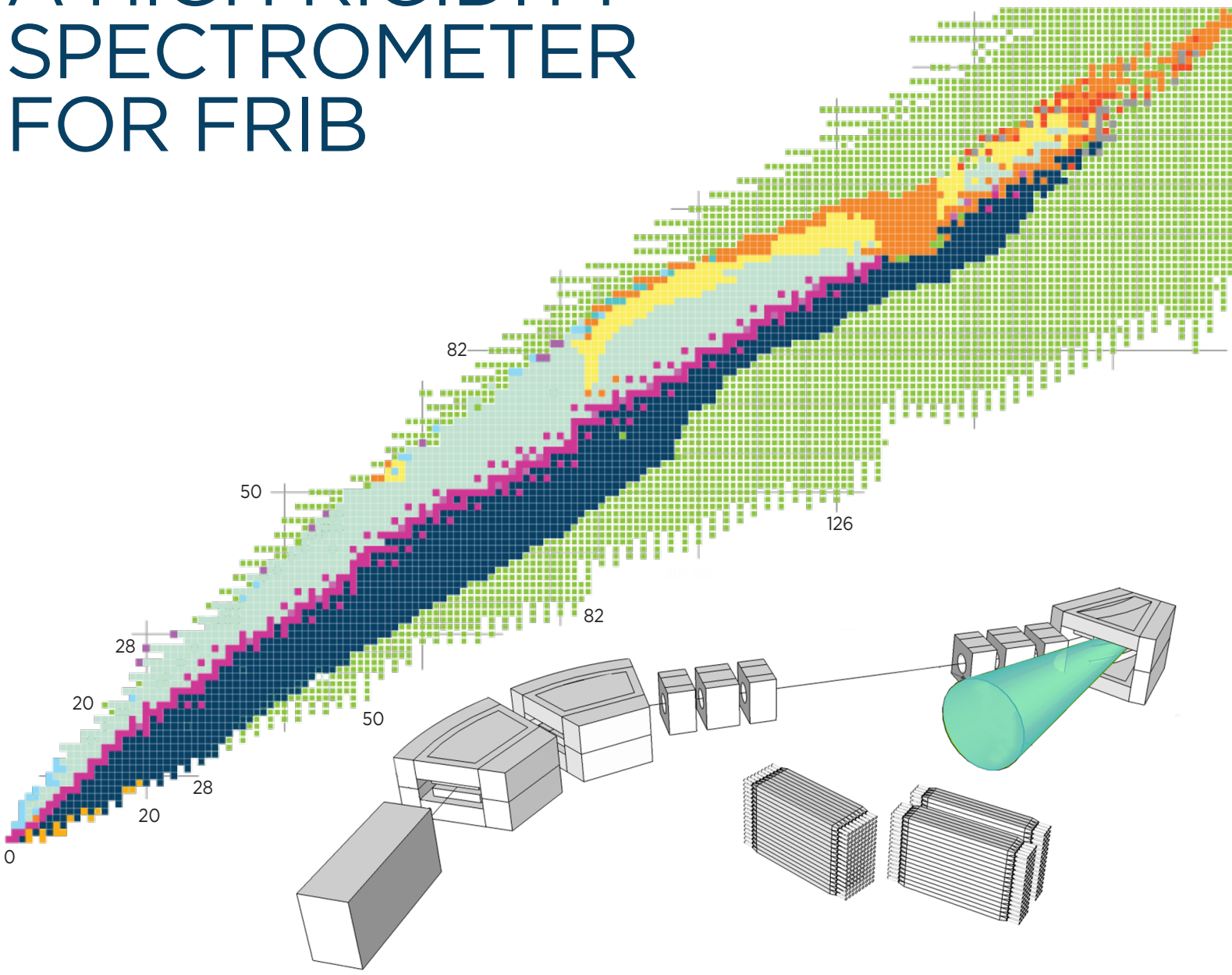

Table of Contents

A High Rigidity Spectrometer for FRIB

1. Introduction and executive summary

The Facility for Rare-Isotope Beams (FRIB) will be the world's premier rare-isotope beam facility, producing a very large fraction (~80%) of the isotopes predicted to exist [ERL12]. The scientific community is preparing to make full use of the capabilities of FRIB, which includes the development of state-of-the-art experimental tools that enable experiments with the highest scientific impact and that allow for exploration of the furthest areas of "terra incognita" on the chart of nuclei.

This whitepaper presents the scientific case for the construction of a High Rigidity Spectrometer (HRS) at FRIB, which will be the centerpiece experimental tool of the FRIB fast-beam program. By enabling experiments with beams of rare isotopes produced at energies at which the production rate by fast fragmentation is maximal (170-200 MeV/u), and that are transported with minimal losses from the FRIB fragment separator to the HRS, an ideal environment for achieving many of the key scientific goals of the FRIB community is created. At the HRS, experiments with the most neutron-rich, short-lived, rare-isotope beams produced at FRIB will be possible. Besides ensuring these optimal running conditions, the HRS will expand the beam energy range available for experiments, including those that utilize other major experimental equipment items, such as the Gamma-Ray Energy Tracking Array (GRETA) and the Modular-Neutron Array (MoNA-LISA) can be performed at FRIB.

In the recent NRC decadal study "Nuclear physics: Exploring the Heart of Matter" [NRC13], four overarching challenges for the field were outlined, similar to those phrased earlier in the NSAC 2007 Long Range Plan [LRP07]. These 4 questions, related to nuclear structure, nuclear astrophysics, tests of fundamental symmetries and interactions and applications of isotopes, are listed in table 1 and connected to 17 specific benchmarks set by the NSAC RIB Task Force [RIB07] that measure capability to perform rare-isotope research. The scientific motivations laid out in this whitepaper for the HRS map closely on these benchmarks, as indicated by the relevant section marked in table 1. Thirteen out of the 17 benchmarks are covered. Some of the benchmarks are quite tightly defined: for example, the HRS will not be used for studies of the atomic Electric Dipole Moment (EDM), but certain measurements with the HRS closely relate to fundamental interactions, such as charge-exchange experiments used for reducing the uncertainties in the calculation of nuclear matrix elements of importance for neutrino-less double-β decay. Certain astrophysical processes, such as novae, were not explicitly listed as benchmark,

but relevant information about critical thermonuclear reactions can be obtained in experiments with the HRS, as discussed in the whitepaper.

From the mapping in table 1, it is clear that the scientific objectives of the experimental programs with the HRS are very broad and of high-impact. In addition, a large fraction of the required techniques for performing the programs with the HRS have been developed in experiments at the S800 spectrograph and sweeper magnet at the National Superconducting Cyclotron Laboratory (NSCL). These programs are, and have been, highly successful, and comprise about half of the scientific program of NSCL. Like the experiments with the S800 and the sweeper magnet, experiments at the HRS will often be run in combination with other state-of-the-art experimental equipment, including the Gamma Ray Energy Track Array (GRETA) and the modular neutron array MoNA-LISA. As discussed in the whitepaper, such combined experiments will strongly enhance the scientific output of the program.

TABLE 1 FOUR OVERARCHING QUESTIONS OF THE NRC DECADAL STUDY "NUCLEAR PHYSICS: EXPLORING THE HEART OF MATTER" AND ASSOCIATED BENCHMARKS SET BY NSAC RIB TASK FORCE. THE SECTION NUMBERS REFER TO SECTIONS IN THIS WHITEPAPER THAT SPECIFICALLY REFER TO THESE BENCHMARKS.

How did visible matter come into being and how does it evolve?		How does subatomic matter organize itself and what phenomena emerge?	
Equation of State	3.2,4.1,4.2,4.4-4.6	Shell structure	2.1-2.9,3.1
r-process	4.3	Superheavies	-
15O(α,γ)	-	Skins	4.1,4.2,4.5,4.6
^{59}Fe Supernovae	-	Pairing	-
Mass surface	5.1	Symmetries	2.6
rp-process	2.3,2.6	Limits of Stability	2.1, 2.2,2.6
weak interactions	2.7,4.6,5.3	Weakly bound nuclei	2.1
		Mass surface	5.1
Are the fundamental interactions that are basic to the structure of matter fully understood?		**How can the knowledge and technological progress provided by nuclear physics best be used to benefit society?**	
Atomic EDM		Medical	
		Stewardship	2.8

The main distinguishing feature of the HRS compared to the existing S800 spectrograph and sweeper magnet is the increased charged-particle bending power of the HRS. The foreseen maximum magnetic rigidity (Bρ) of the HRS (~8 Tm) is about double that of the S800 and sweeper magnet, and is ideally matched to the beam energies (~170-200

MeV/u) at which the yield for rare-isotope beams at FRIB is maximal. This is illustrated in Fig. 1.1, which displays the magnetic rigidity at which the maximum beam intensity is achieved at FRIB across the chart of nuclei. Except for the nuclei along the proton dripline, the required magnetic rigidities exceed the values accessible by the existing devices. In particular for the most neutron-rich nuclei, the impact is very strong, as the maximum rare-isotope yields are achieved between 5 and 8 Tm, including for nuclei on the astrophysical r-process path, which is also indicated in the figure. Estimated loss factors due to not being able to run experiments at the optimal magnetic rigidity, but having to slow down the produced rare isotope beams to energies manageable by the existing devices range from a factor of 2 to 5, with the larger loss factors occurring in the more neutron-rich regions. Additional gains in reaction rates are achieved at the higher beam energies because thicker reaction targets can be used at the experimental station and because problems with charge-state contaminations decrease at the higher beam energies (see Fig. 1.2). In addition, it is envisioned that the beam line that transports rare-isotopes beams from the FRIB fragment separator to the HRS will be designed with a large acceptance to ensure the highest transmission. All-in-all, estimated effective intensity gains of up to a factor of 10 can be achieved with the HRS compared to a situation where existing NSCL devices would be used. Such a factor has a tremendous impact on the scientific program, in particular in neutron-rich regions far from stability. To illustrate this, Fig. 1.1 also contains contour lines for maximum reaction rates achieved. In the most neutron-rich regions, expected rates drop rapidly and eventually fall below levels of 1 particle/s. Of course, many of the highest-impact experiments will utilize beams of isotopes in these neutron-rich regions and beam intensities will be the main limitation of the experimental count rate. Therefore, scientific output more-or-less directly scales with the gain factor achieved by running at the higher rigidity.

A second important motivation for the construction of a spectrometer that can operate at high rigidities, is that experiments at higher beam energies open up additional scientific opportunities not available at lower beam energies. Such additional opportunities are also discussed in this whitepaper.

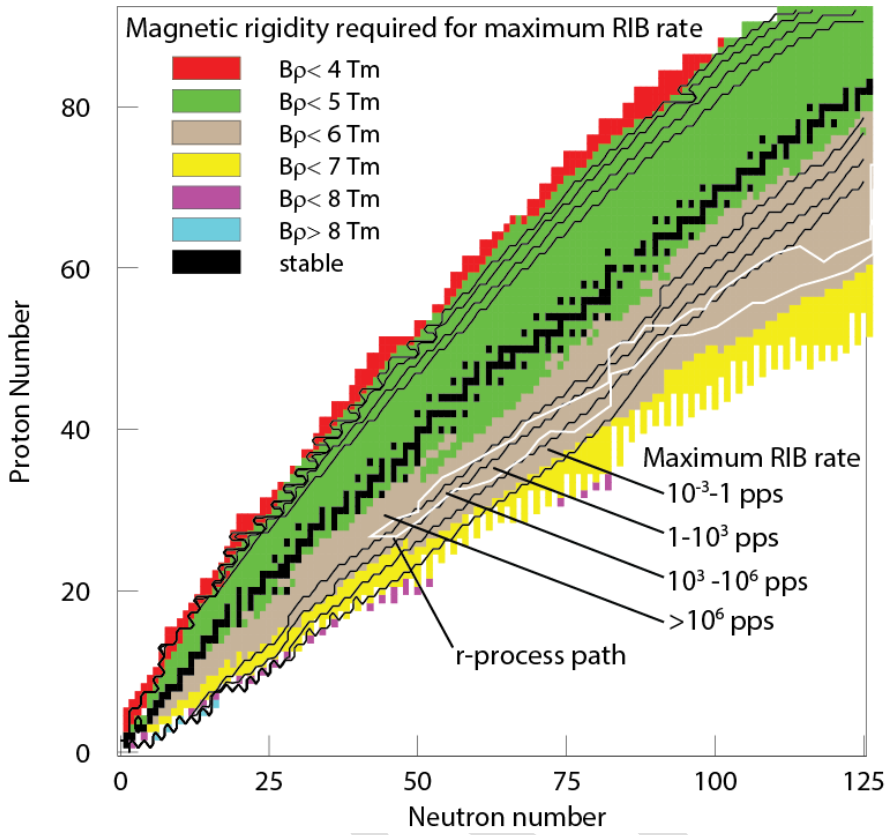

Fig. 1.1 Chart of the nuclei indicating in color the magnetic rigidities (Bρ) at which the maximum beam intensity for the production of the rare isotopes is achieved. The solid black lines indicate contours for the rare-isotope production rate. The white line indicates the astrophysical r-process path.

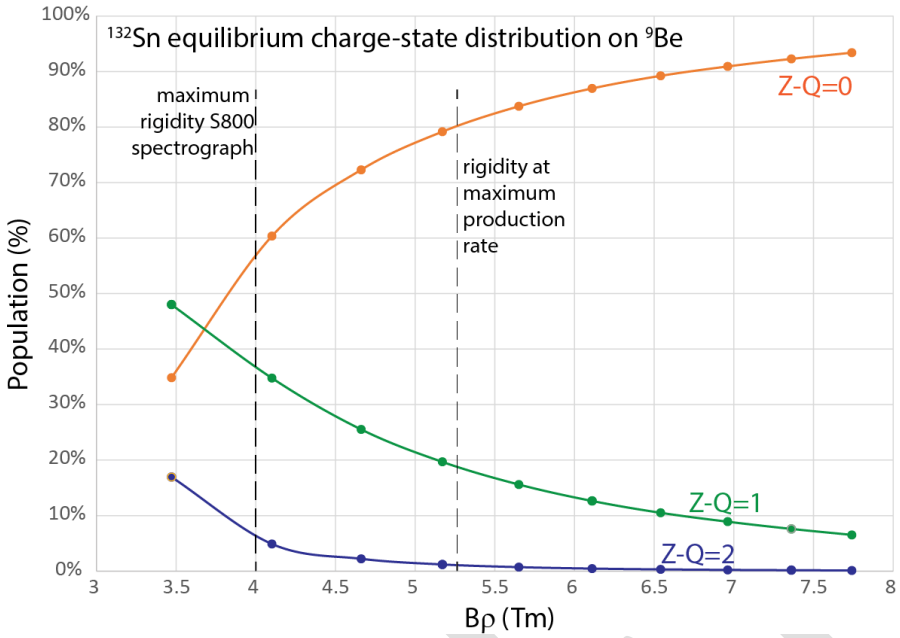

Fig. 1.2 Equilibrium charge-state distribution after a ^{9}Be target for a fully stripped ^{132}Sn incoming beam at 170 MeV/u, calculated by using the code GLOBAL [SCH98]. Z-Q=0 indicates fully-stripped ^{132}Sn after the target, Z-Q=1 and Z-Q=2 indicates that one or two electrons have been picked up, respectively. The maximum rigidity of the existing S800 spectrometer is indicated, as well as the rigidity at which the maximum beam intensity for ^{132}Sn is achieved at FRIB and at which the proposed HRS could easily be used to perform experiments. Clearly, at a rigidity around 4 Tm, about half of events produced in a reaction target placed at the spectrometer are lost because events are produced in different charge-states. At a rigidity of 5.25 Tm, the percentage of events not populating the fully stripped ejectile is reduced to 20%.

The pre-conceptual design parameters of the HRS (see section 6) were chosen based on the needs for the scientific program discussed in this whitepaper. Construction of the HRS would eliminate the need for the existing sweeper magnet used in experiments with MoNA-LISA. Instead, MoNA-LISA would be moved to the experimental area of the HRS. There will be a remaining need for experiments at the S800 spectrometer, as the energy resolution achievable with the S800 is exceptionally good, and certain experiments require that very high resolution, which would be very expensive to achieve at the magnetic rigidities foreseen for the HRS. In addition, it is important to maintain some flexibility in running options with fast rare-isotope beams, as the demand will likely be high (at NSCL, about half of the program is performed at the S800 spectrometer and sweeper magnet).

Over the course of the years the FRIB Scientific Advisory Committee has provided extremely positive feedback to the HRS working about the plans for the construction of the HRS:

"The SAC viewed the science addressed in your submission as having the highest scientific priority and this was communicated to the FRIB Laboratory Director. The SAC views the activity of your group as central to the FRIB mission and encourages your continued actions. The HRS is one of the flagship projects at FRIB. To facilitate the fast beam programs, the HRS is designed to be coupled with detectors necessary for experiments enabling techniques such as missing-mass, in-beam gamma and invariant mass in inverse reactions…The HRS is necessary to conduct the scientific mission of FRIB."

This whitepaper was written on the basis of discussions held over several years within the HRS working group at a number of different venues, most recently (July 2014) at a dedicated workshop in which more than 60 participants from 19 US institutions (and 5 non-US institutions) participated. Several more contributed to specific sections of this document. The HRS working group conveners and the contributors to the latest workshop and this document are listed at the end of this whitepaper.

In the following, the scientific motivations are discussed, grouped by "Evolution of nuclear structure", "Benchmarking direct reactions", "Aspects of Nuclear Matter" and "Nuclear Astrophysics". The last section provides details of the pre-conceptual design of the HRS, as well as a cost estimate and timeline for the construction of the device.

2. Evolution of nuclear structure

Near stability, the nuclear shell structure is well understood. Shell gaps, occurring at the fillings of single-particle orbitals with a magic number of nucleons, set the model spaces required for a quantitative description of the nucleus. With the average nuclear potential well parameterized for stable nuclei, phenomenological frameworks describe the majority of experimental observables. However, away from stability, decreasing nucleon binding together with the large proton-to-neutron asymmetry lead to modifications of the nuclear potential and the spin-isospin components of the nucleon-nucleon interaction fuel changes to the single-particle energies. Together with the increased role of a variety of many-body correlations, these modifications of the single-particle structure result in the disappearance of magic numbers established close to stability and the appearance of new shell gaps. Beyond these changes to the shell structure, which can at least be partially captured within phenomenological approaches, theoretical descriptions of nuclei are aiming towards a more microscopic picture and even ab-initio calculations. In light systems, such as the Z=6 and Z=8 isotopes, where ab-initio calculations have been possible for several years, microscopic calculations have shown the need to include forces beyond two-body interactions, with an accurate description of basic nuclear properties such as binding energies or masses requiring the inclusion of three-body nucleon (3N) interactions [OTS10,HAM13]. Experimental information on single-

particle and collective degrees of freedom is crucial to benchmark the rapidly developing nuclear structure theories in the quest for a predictive model of nuclei. Unique opportunities arise along the N=Z line, where T_z=0 proton-neutron correlations can be studied with unprecedented clarity. The N=Z line comes close to the proton dripline around the alleged double-magic N=Z nucleus ^{100}Sn, where spectroscopic information is still scarce. In medium mass nuclei with N<Z, the most exotic partner of mirror nuclei is located at the proton dripline, where the effect of weak binding and the continuum on isospin-breaking effects can be explored in addition to aspects of the proton-neutron interaction.

Charge-exchange reactions are a unique tool to study the spin-isospin response of nuclei. In contrast to β decay, in which only nuclear states in the limited Q-value window are accessible, charge-exchange reactions probe the entire response function, including the giant-resonance region. Gamow-Teller distributions from charge-exchange reactions provide a complementary tool to track the evolution of nuclear structure in exotic nuclei.

Towards the heaviest nuclei, more than 75 years after its discovery, the process of fission is still not fully understood. Finally, present-generation computational power allows attempting the development of predictive models of this very complex many-body process. For this, information is necessary on the very details of the nuclear structure of the fission fragments, where basic information as, for example, the low-lying level densities are presently taken from statistical models that do not include the effects of the volatile, changing shell structure.

Fast rare-isotope projectiles produced in-flight by fragmentation or fission of fast primary beams allow for in-beam spectroscopy measurements at rates of a few particles per second or less by restoring luminosity through the use of thick reaction targets. A variety of fast-beam experimental techniques can be used to track the evolution of nuclear structure in the quest for a comprehensive model of the atomic nucleus with predictive power also in the exotic regime. For example, in-beam spectroscopy using direct reactions is sensitive to single-particle structure and inelastic scattering processes probe collective degrees of freedom, providing crucial and complementary information on the nuclear many-body system. Excited-state lifetime measurements enable the model-independent precision determination of transition matrix elements between nuclear states. Delayed β-decay or isomer spectroscopy of residues implanted after a reaction affords unique and efficient final-state identification in some cases.

At FRIB, these parts of the nuclear science program will require in-beam spectroscopy arrays, like MoNA-LISA and a Si array for neutron- or proton-unbound states, respectively, and GRETA for bound states, coupled to the HRS. A versatile focal-plane design for the

HRS is planned to enable decay spectroscopy of rare reaction residues. The following sections highlight example science programs aimed at the study of the evolution of nuclear structure at the HRS.

2.1. At the limits of the nuclear chart - Nuclear structure beyond the neutron dripline

Radioactive ion beam facilities have provided the unique opportunity to explore nuclear matter at the limits of stability [BAU12]. When moving away from the valley of stability towards the proton or neutron driplines, the standard shell model has been shown to break down, resulting in new phenomena amplified by weak binding and the proximity of the continuum [PFU12, THO04, HAN01, BRO01]. Measurements of neutron-unbound nuclei allow for the exploration of nuclear structure beyond the neutron dripline and can provide stringent constraints for nuclear theory [BAU12].

The Modular Neutron Array [LUT03, BAU05] and the Large multi-Institutional Scintillator Array [MRI09] (MoNA-LISA) coupled to the 4-Tm Sweeper Magnet have been used to successfully explore a wide range of neutron-unbound states and nuclei at the NSCL through invariant-mass spectroscopy. The current MoNA-LISA-Sweeper setup is shown below in Fig. 2.1. Typically, a one- or two-proton knockout reaction from a radioactive beam is used to populate an unbound state or nucleus which then immediately (within ~10-21 seconds) decays into a charged particle (the projectile-like decay daughter) and a neutron. The charged remnant is deflected into a suite of detectors by the Sweeper magnet while the neutrons, unaffected by the magnetic field, travel forward into the MoNA and LISA neutron arrays. Since the momentum, angle, and mass of each particle in the decay process are measured, the Lorentz vectors are known and the invariant mass of the decaying system can be reconstructed (also referred to as the decay energy).

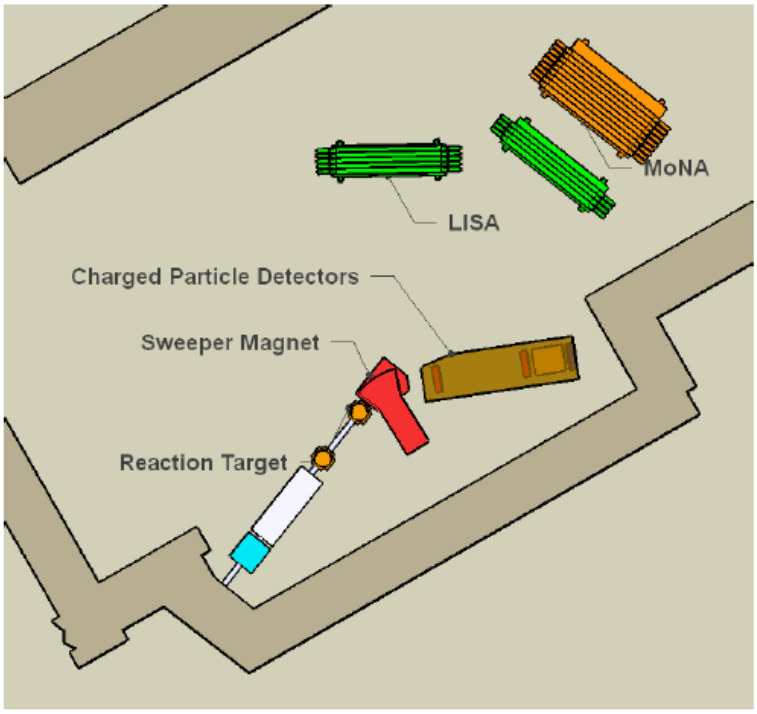

Fig. 2.1 Schematic illustration of the existing MoNA-LISA-Sweeper setup at NSCL.

Since the implementation of MoNA and the Sweeper at NSCL over a decade ago, neutron-unbound states or nuclei primarily in the light-mass region between helium [DEN08] and fluorine [CHR12] were investigated. A few of the recent highlights from the research program are listed below and will serve as motivation for the future studies expected to be carried out at FRIB:

- *Evolution of shell structure away from stability:* The neutron-unbound states of ^{23,24}O [SCH07,HOF09,HOF11] and the unbound nuclei ^{25,26}O [HOF08,LUN12] were investigated using the MoNA-Sweeper setup. The results demonstrated the presence of "new" magic numbers at neutron numbers N=14 and N=16 for these exotic neutron-rich oxygen isotopes.
- *Two-neutron decays:* The pairing interaction increases the stability of even-neutron nuclei also beyond the dripline and these nuclei might be bound with respect to one-neutron emission but unbound with respect to two-neutron emission. Techniques to reconstruct these two-neutron decays have been developed and led to the discovery of the ground states of ^{13}Li [KOH13], ^{16}Be [SPY12], and ^{26}O [LUN12].
- *3-body correlations:* Along with measurements of the decay energy of the two-neutron unbound state/nuclei, the correlations of the 3-body system have also been measured. The results have consistently demonstrated that the neutrons are

emitted with a strong "dineutron-like" correlation [SPY12,KOH13a]. With improved theoretical calculations, these 3-body correlations will provide a link to the wave function of the unbound nucleus.

- *New phenomena:* In moving away from stability, new phenomena can emerge due to the drastic changes in the binding energy and shell structure of the nuclei. One example is ^{26}O, which provided the first evidence for two-neutron radioactivity [KOH13a].

The MoNA-LISA research program outlined above will be an important aspect for the continued studies of neutron-rich nuclei at FRIB. The increased rare-isotope beam rates of FRIB will allow for new unbound nuclei and states to be reached that are currently unavailable at the NSCL. Fig. 2.2 shows the range of unbound nuclei and nuclei with low-energy unbound states that will be accessible at FRIB using the invariant-mass spectroscopy technique using MoNA-LISA. This will greatly expand the current knowledge about the structure and properties of these medium-mass neutron-rich nuclei in the continuum.

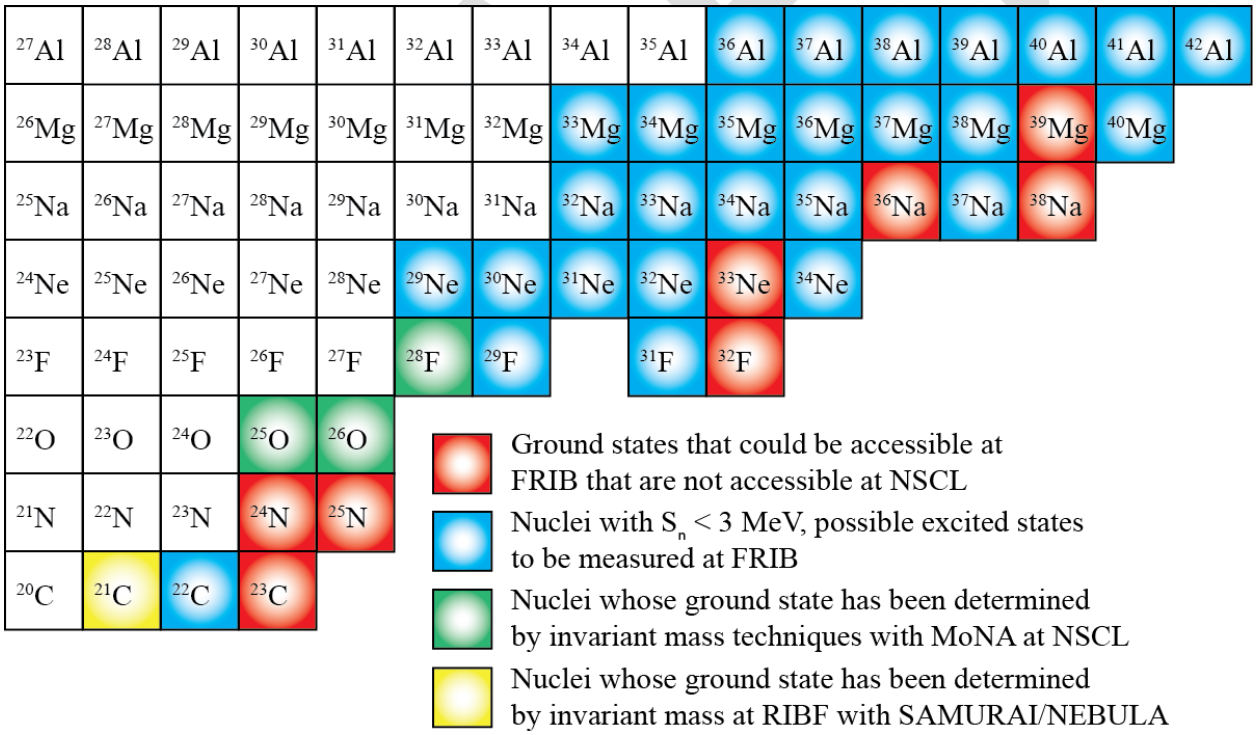

Fig. 2.2 The range of unbound nuclei and stable nuclei with low-energy unbound states that will be accessible at FRIB using the invariant-mass spectroscopy technique using MoNA-LISA

This is an especially interesting part of the nuclear chart as it extends to the neutron-rich exit of the so-called "island of inversion", a region of dramatic shell evolution that allows tracking shell-structure modifications into the continuum. While the studies so far

concentrated on the evolution within the sd-shell, FRIB will allow to access information within the pf-shell. The single-particle energies in the pf-shell are very similar, resulting in the shallow decrease of the one- and two-neutron separation energies as the shell is filled. Thus, a wide range of isotopes lie close to the dripline making them ideal candidates to be studied by their neutron decay (see Fig. 2.2). This broad access to new mass regions will also allow identifying additional cases of the rare, new phenomenon of two-neutron radioactivity. The increase of the angular momentum barrier in the pf-shell compared to the sd-shell also increases the decay-energy window where this exotic decay mode could be observed.

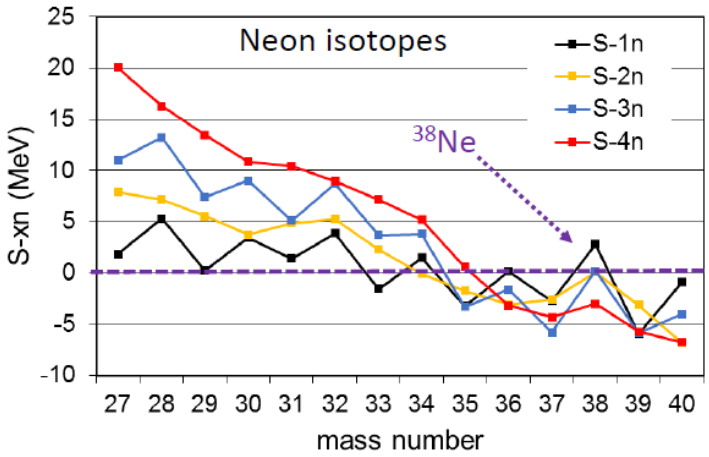

Fig. 2.3: Multiple neutron separation energies S_{xn} (with x = 1-4) for neutron-rich neon isotopes predicted by the FRDM [MOE95]. ^{38}Ne is predicted to be a 4-neutron emitter.

One interesting possibility in this very neutron-rich region of the pf-shell is the presence of 4-neutron emitters. For example, the finite range droplet model (FRDM) [Moe95] predicts ^{38}Ne and ^{44}Mg to be unbound with respect to the emission of four neutrons but bound with respect to the emission of one, two, or three neutrons as shown in Fig. 2.3. Thus, these nuclei would decay by the simultaneous emission of four-neutrons.

While FRIB will provide increased rare-isotope beam rates, providing first access to the nuclei shown in Fig. 2.2 with the technique of invariant mass spectroscopy, the current 4-Tm Sweeper magnet used with MoNA-LISA is not adequate to perform these studies. The fact that the Sweeper setup is comprised of a single dipole magnet instead of a spectrometer limits its mass resolution and will not allow for studies of heavier nuclei. Additionally, the magnetic rigidity, Bρ, of the Sweeper magnet is insufficient to bend the projectile-like decay remnants in invariant mass spectroscopy at FRIB's beam energies. For example, a 200 MeV/u beam of ^{42}Al projectiles will have a Bρ of about 7 Tm when produced to achieve the highest yield for the most effective measurements. Therefore,

a high-rigidity spectrometer is necessary to allow the continued study of the most exotic neutron-rich nuclei through invariant mass spectroscopy. Finally, the gap of the present Sweeper magnet is only 14 cm, which effectively limits the acceptance for detecting and reconstructing neutron decay energies to less than about 2 MeV.

2.2. Single-particle structure and collectivity from prompt in-beam γ-ray spectroscopy

The often surprising properties of nuclei beyond the valley of β stability have prompted extensive experimental and theoretical studies aimed at identifying the driving forces behind the dramatic changes in nuclear structure that are encountered in rare isotopes. Many of the most exotic nuclear species are available for experiments as fast ion beams with velocities exceeding 30% of the speed of light. Intermediate-energy Coulomb excitation, inelastic proton scattering and nucleon removal reactions have evolved from novel techniques to versatile spectroscopic tools that provide information on the single-particle structure and on collective degrees of freedom in nuclei accessible for experiments at beam rates of a few ions/s. The following subsections outline two types of measurement in interesting regions of the nuclear chart that serve as examples of broad programs that are expected to be pursued at FRIB across all mass regions.

I. The chain of Calcium isotopes studied with nucleon knockout

The proton-closed shell calcium isotopes with Z=20 present a unique laboratory for studying the evolution of structure with increased neutron number. Within this single isotopic chain are some of the clearest examples to date of changing single-particle energies as a result of the spin-isospin component of the nucleon-nucleon interaction, namely the appearance of new sub-shell gaps at N=32 and 34 [HUC85, GAD06, STE13]. In addition, recent microscopic calculations [HOL12, HOL14] have highlighted the Ca isotopes as a region of the chart in which to test the role of three-nucleon forces in providing a more complete microscopic description of the atomic nucleus.

FRIB will provide access along the $_{20}$Ca isotopic chain with unparalleled reach, allowing detailed spectroscopy as far as N=36, and first spectroscopy out to ^{60}Ca. Stringent tests of microscopic calculations will be possible using direct nucleon knockout reactions to study the occupation of single-particle states as a function of neutron number. However, to fully realize the full extent of scientific reach provided by FRIB, it will be critical to have the tools to optimize use of these beams. Fast beams of neutron-rich Ca isotopes will have magnetic rigidities in the range of 5.5 Tm to 6.5 Tm and a high-rigidity spectrometer will be critical for nucleon knockout experiments. The combination of the HRS coupled to a gamma-ray spectrometer such as GRETA will allow detailed prompt gamma

spectroscopy at the very limits of FRIB reach, and will be a cornerstone of experimental equipment for fast-beam research at FRIB.

II. Shell structure and collectivity near ^{40}Mg

An example of single particle shell evolution which has been both a theoretical and experimental focus in recent years is the quenching of the *N*=28 shell gap below the $_{20}$Ca isotopes. With decreased occupancy of the proton $d_{3/2}$ orbital, the neutron *f* orbitals are essentially pushed closer in energy, while the spacing between proton orbitals is simultaneously reduced. The narrowed single-particle orbital spacings leads to the development of $\Delta l = 2$ quadrupole excitations for both protons and neutrons, resulting in well-developed deformation along *N*=28. Recent spectroscopic work has further shown that, at least in the $_{12}$Mg isotopes, deformation extends all the way from the island of inversion near *N*=20 to ^{40}Mg at *N*=28 [DOO13, CRA14]. However, the quantification of the extent of deformation, and an experimental confirmation of the evolving single-particle states leading to this deformation requires the intensities that will only be achieved with FRIB's fast beams.

Proton and neutron knockout measurements in this region will provide the spectroscopic information to fully map out the changing proton and neutron single-particle energies and nucleon occupancies in this region, while Coulomb excitation and lifetime measurements will provide a quantification of the degree of collectivity. However, these experiments will be among the most demanding in terms of a spectrometer. FRIB beams in the region of ^{40}Mg will reach magnetic rigidities of just over 7 Tm, and with intensities of as low as a few particles per second, experiments will be possible only with a high-rigidity spectrometer. This is another region of the nuclear chart in which the combination of GRETA and the HRS will provide a truly unique scientific opportunity.

2.3. Fingerprints of shell evolution with isomer studies

An experimental challenge for the powerful reaction studies proposed for medium-heavy to heavy nuclei is the occurrence of long-lived isomeric states in the reaction products as well as in the incoming projectile beam. In fact, these isomeric states are often a direct finger print of shell evolution and originate from the hindered decays of states that cross a shell gap to intrude the normal-order single-particle structure.

In knockout reactions, for example, an important observable is the parallel momentum distribution of the projectile-like knockout residue which provides the orbital angular momentum value of the removed nucleon and thus detailed information on the nuclear wave function. For the residue ground state, this distribution is usually obtained by subtracting from the from the inclusive parallel momentum distribution the appropriately scaled momentum distributions for events where a prompt γ-ray transition to the ground

state was detected. If isomers are present in the reaction product, this is not possible anymore and the so-obtained momentum distribution will consist of events where the residue was left in the ground state or an isomeric state. Furthermore, the level scheme extracted from prompt γ-ray measurements can be wrong, if transitions feeding isomeric states are mistaken as ground-state transitions. Depending on the beam energy, even level lifetimes of the order of several ns can lead to systematic errors in the measurements. In order to avoid these complications and to identify and characterize the important isomeric states, a new approach of tagging and identifying the population of isomeric states in the reaction products has been developed recently and was first applied at the S800 spectrograph at NSCL [WIM14]. After identification of the reaction products by mass and charge in the focal-plane detector system, the ions were implanted into a 6.35 mm thick aluminum plate. γ-ray transitions following isomeric as well as beta decay were measured in a CsI(Na) array placed behind the stopping plate. The decay of isomeric states with lifetimes between ~100 ns and several ms has been observed and event-by-event linked to the implantation event. With this, the population of isomeric intruder states could be quantified for the first time in the key region around N=40 in the vicinity of ^{68}Ni and valuable nuclear structure information was obtained on the presence of the intruder neutron $g_{9/2}$ orbital and its occupation by neutrons.

At FRIB, nuclei in the vicinity of the key nucleus ^{78}Ni will become available for powerful direct-reaction studies with GRETA at the HRS. Nuclei around ^{78}Ni (N=50, Z=28) exhibit a large number of observed and predicted isomeric states. These can, for example, result from the large difference in total angular momentum between the active orbitals at the Fermi surface, the neutron $g_{9/2}$ and the $s_{1/2}$ (above N=50) and $p_{1/2}$ (below the N=40 sub-shell gap) orbits (single-particle isomers) [GRZ98]. Since these states represent almost pure configurations, reactions from or to isomers yield important information on the single-particle energies and their evolution around the presumed doubly magic ^{78}Ni.

Isomeric states are also prominent in regions of astrophysical interest for the r-process around the magic neutron number N = 82. In this region, seniority and single-particle isomers have been predicted and observed (see for example [WAT13]). The structure of nuclei below ^{132}Sn has a significant influence on the timescale and the location of the r-process path. Spectroscopic information from reactions on Cd or Pd nuclei below the doubly-magic shell closure will therefor provide important constraints for astrophysics calculations.

On the proton-rich side of the valley of stability, in the region around ^{100}Sn, where the rp-process is proposed to end, several isomeric levels have been observed and are predicted [GRA06]. Spectroscopic studies of nuclei in this region are not possible without experimental information on the population of isomeric states in the reaction products as

well as on the isomeric content in the projectile beam itself. In-beam experiments with fast radioactive ion beams at FRIB require detection of delayed γ-ray or conversion electrons in the focal plane of the spectrometer. Good energy and time resolution as well as large areal coverage are desired. Therefore, a detector array based on scintillator crystals is best suited for this. The detection efficiency can be maximized by implanting the ions directly into the scintillator material. $LaBr_3$(Ce) seems to provide the best properties for the proposed application, but new materials such as $CeBr_3$ exhibit also good timing and energy resolution properties.

2.4. Excited-state lifetimes as indicators of shape and shell evolution

Excited-state lifetime measurements provide a model-independent approach to determine transition matrix elements. Recently, a new plunger device TRIPLEX (TRIple PLunger for EXotic beams) optimized for recoil-distance Doppler-shift measurements with fast rare-isotope beams has been developed at NSCL in collaboration with Cologne University, Germany. The device uses three thin metal foils separated by very precisely known distances. In this approach, Coulomb excitation or knockout reactions are used to populate excited states in the exotic, projectile-like reaction residues of interest. These excited nuclei γ decay in flight after traveling a distance related to their excited-state lifetimes. Two degraders are positioned downstream of the target to reduce the velocity of the ions at precisely known distances from the target. As a consequence, γ rays emitted behind each foil will have different Doppler shifts. The lifetime of the state can then be determined using relative γ-ray yields measured at different foil separations. A notable advantage of this method is that transition matrix elements can be obtained directly from the measured lifetimes without employing reaction analyses. This approach is applicable to different transition modes such as E1, M1 and E2 excitations if the level lifetimes are within measurable ranges of about one picosecond to one nanosecond.

At the HRS, excited-state lifetime measurements will be performed using rare-isotope beams provided by FRIB and the advanced γ-ray tracking array GRETA. In addition to the unmatched access to exotic nuclei out of reach at present, the higher beam energies - relative to NSCL beam energies - will increase the experimental feasibility and reach of the recoil-distance measurements based on the multi-foil plunger scheme, allowing for efficient lifetime measurements in the most exotic regime where beam intensities or reaction cross sections are very small.

Recently, shape coexistence phenomena induced by shell evolution far from stability attracted great interest. Normal and intruder configurations compete strongly in neutron-rich nuclei close to conventional magic numbers, which results in the appearance of two or more different intrinsic shapes and associated band structure at low excitation

energies. Such phenomena are predicted to occur in the vicinity of ^{32}Mg (Fig. 2.4) and ^{68}Ni (Fig. 2.5), where experimental information is still limited for higher-lying excited states beyond the yrast excitations. Critical excited-state lifetime measurements for the 2^+ and 4^+ states in such higher-lying bands in neutron-rich nuclei can be performed at the HRS by combining intense rare-isotope beams and the powerful GRETA array. Gamma-gamma coincidence and delayed γ-coincidence measurements can be applied to selectively study excited states of interest in key regions across the nuclear chart. Through the measurement of transition rates for higher-lying states, the excited band character as well as associated shell configurations can be experimentally investigated for the first time in the most exotic nuclei. In this way, modification of the shell structure can be probed at the HRS as a function of spin, isospin, and excitation energy, paving the way for a complete understanding of the shell evolution in neutron-rich nuclei.

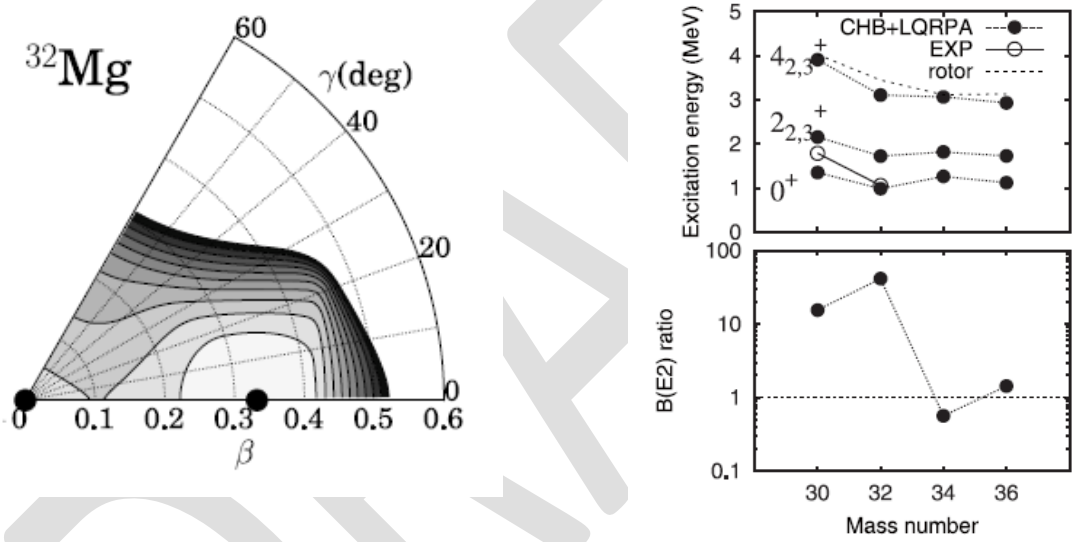

Fig. 2.4 Example 1 from [HIN12]: Potential energy surface of ^{32}Mg as function of the beta and gamma deformation parameters (left) and evolution of excitation energy and B(E2) ratio across the Mg mass number, signaling the sudden change between A=32 and 34 (right).

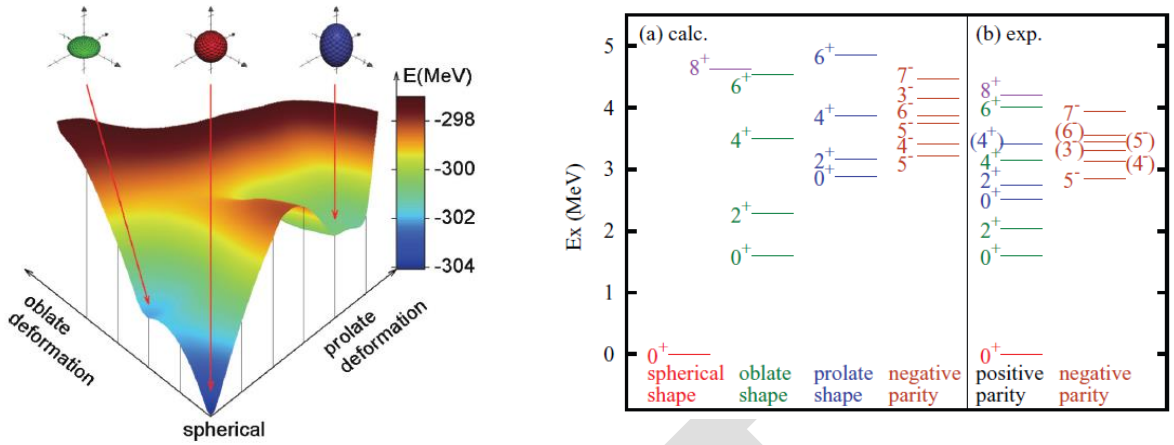

Fig. 2.5 Example 2 from [SUC14,TSU14]: Potential energy surface as calculated by the Monte Carlos shell Model for the N=40 nucleus ^{68}Ni (left) and level scheme associated with the three coexisting shapes. Transition strengths measurements will reveal the band structures and their interconnections.

2.5. Inelastic proton scattering as a probe of the proton-neutron degree of freedom

Proton inelastic scattering has been proven to be a powerful tool in the investigation of the proton–neutron degree of freedom in nuclear structure physics [ALA96]. In the proximity of a closed neutron or proton shell, the quantification of proton and neutron contributions to a transition between two nuclear states provides crucial information on the relative importance of valence nucleons and the core. If the core was inert, low-lying excitations would be entirely dominated by contributions of the valence species.

In inelastic proton scattering, collective modes are preferentially excited. In even–even nuclei these are most often the lowest-lying 2^+ and 3^- excited states. Hadronic scattering is complementary to Coulomb excitation since the electromagnetic (Coulomb) excitation interrogates the proton transition matrix element, M_p, only, while inelastic proton scattering is a probe with mixed sensitivity to protons and neutrons.

Deformation lengths deduced for excited states populated in proton scattering can be combined with electromagnetic reduced transition probabilities, B(E2), from Coulomb excitation or excited-state lifetime measurements, to determine the ratio of neutron to proton transition matrix elements M_n/M_p [BER83]. This ratio, for collective 2^+ states in even-even nuclei, is a sensitive indicator of a shell closure. In single-closed-shell nuclei, M_n/M_p has been shown to be more sensitive to shell-model effective charges than *B(E2)* values alone [RIL05]. Hence, inverse-kinematics proton scattering will be an important tool for mapping the evolution of shell structure for some of the most exotic nuclei provided by FRIB.

Proton angular distribution measurements made with thin targets and particle telescopes (see for example Refs. [MAR99,SCH00]) typically require beam intensities on the order of 10^4 particles per second (pps), while thick-target inelastic scattering measurements (for example Refs. [RIL05,CAM06,TAK09,SUZ13]), in which γ rays are detected instead of scattered protons can be performed accurately and including feeding corrections with beam intensities as low as 10 particles per second (pps). These two approaches have both been used at the NSCL. Proton angular distributions from elastic scattering enable a direct determination of the optical potential parameters used to extract deformation lengths of inelastic excitations. Thick-target experiments enable measurements of the most exotic, lowest-intensity beams but they yield no elastic scattering information and instead must rely on extrapolations of empirical optical potentials [KON03]. The determination of optical potential parameters from proton elastic scattering will be crucial at the higher beam energies of FRIB and at the extreme neutron/proton asymmetries we will explore with FRIB.

It is planned to pursue a program of inverse-kinematics proton scattering measurements with the HRS at FRIB, making thick-target γ-ray measurements with the GRETA γ-ray tracking array and a liquid-hydrogen target, of the most exotic, lowest intensity beams (10 pps), including ^{100}Sn and ^{132}Sn at $Z = 50$, the $N = 82$ nucleus ^{128}Pd, ^{50}Ni and ^{78}Ni at $Z = 28$, ^{58}Ca *at* $Z = 20$, and the $N = 28$ nucleus ^{40}Mg, for example. Beam intensities of the nearest even-even neighbors of these extreme cases are predicted to be at or above the 10^4 pps needed to perform proton angular distribution measurements. It is anticipated to pursue these measurements using an active-target time projection chamber currently (under development) coupled to the HRS used for the identification and characterization of the scattered projectiles.

2.6. Physics along the N=Z line

Throughout physics, symmetries play a fundamental role in our basic understanding and theoretical description of nature. In nuclei, the similarity of neutrons and protons combined with the charge independence of the nuclear force is contained in the concept of isospin symmetry. Within the isospin formalism, neutrons and protons are treated — in an analogous manner to spin — as projections of two possible states of the nucleon. The consequences of isospin symmetry are most clearly revealed in nuclei containing equal or nearly equal numbers of protons and neutrons ($N \cong Z$) [WAR06]. For instance, studies of the mirror energy difference (MEDs) in light nuclei [GAD07] and also, increasingly, in heavier mirror nuclei along the $N=Z$ line have yielded important nuclear structure information and generated new questions about isospin non-conserving components [EKM04].

The doubly-magic isotope ^{40}Ca marks the last stable *N*=*Z* nucleus as the preference of heavy stable nuclei is to favor more neutron-rich systems. Consequently, access to the *N*=*Z* line, and particularly nuclei with *N*<*Z*, becomes challenging. With increasing mass, the proton drip line moves closer and neutron-deficient nuclei beyond *N*=*Z* are unbound, including the negative *T*=1/2 mirror partners. The proposed High-Rigidity Spectrometer (HRS), coupled to the high-intensity fast secondary beams provided by FRIB, will allow access to these isotopes and unprecedented science related to

- Isospin symmetry breaking
- Pairing interactions in nuclei
- Shape coexistence
- Nuclear astrophysics and rapid-proton capture (*rp*)-process nucleosynthesis
- Defining the boundaries of the proton drip line
- Spectroscopy and mass measurements of unbound nuclei
- Physics in the vicinity of N=Z=50 ^{100}Sn

With FRIB's intense fast primary beams, the most exotic isotopes out to the proton drip line and up to ^{100}Sn will become available. A few examples of science that could be pursed with the HRS will be discussed in this section.

In recent years studies of mirror nuclei in the $f_{7/2}$ shell have provided information on Coulomb energy difference (CEDs) up to high spin [BEN07]. Many of these experiments have increased their reach in both spin and isospin degrees of freedom though the use of modern advanced γ-ray detector systems coupled to powerful ancillary devices [CED11,NAR07]. Work with radioactive beams has extended these measurements beyond the *N*=*Z* line using the S800 spectrometer coupled to the SeGA γ-ray detection array at NSCL, for instance, to study structure of the exotic isotopes ^{66}Se, ^{65}As [OBE11] and ^{49}Fe, ^{53}Ni [BRO09]. These types of experiments, when performed with a powerful setup such as the HRS combined with GRETA, will allow us to push further into the *fp* shell and out to the most neutron-deficient members of an isobaric multiplet. In particular, measurements of the *T*=1/2 mirror pairs from ^{70}Kr and approaching ^{100}Sn will be possible to study in detail, yielding the most complete data yet at the most extreme limits of the *N*=*Z* line.

Little information exists on many short-lived unbound nuclei beyond the proton drip line. While some proton-unbound nuclei can and have been studied through β-delayed proton emission [BLA07], many are only accessible using in-flight decay methods. Experiments which utilize techniques similar to those recently used to study ^{69}Br [ROG11], an unbound nucleus important in the *rp* process, require a spectrometer capable of identifying and measuring the heavy decay residue. The HRS would be a unique high-

resolution tool for resonance spectroscopy of drip-line nuclei which lie along the *N*=*Z* line between rubidium and tin, the properties of which are nearly completely unknown.

2.7. Gamow-Teller strengths as a probe for shell evolution

The extraction of Gamow-Teller strength distributions from intermediate-energy charge-exchange reactions provides an important tool to test theoretical models describing the forces that bind nucleons into nuclei. Gamow-Teller strength distributions are very sensitive to the evolution of nuclear shells in asymmetric systems and thus provide a way to study such evolution that is complementary to ways provided by other techniques. Since Gamow-Teller transitions are associated with spin and isospin transfer, experiments provide a rather direct window into the spin-isospin components of the nucleon-nucleon interaction [OST92,HAR01]. The study of Gamow-Teller transitions extracted from charge-exchange experiments, in combination with those from β-decay experiments, also provide excellent ways to study isospin symmetry [FUJ11].

Because of experimental considerations, charge-exchange experiments on unstable nuclei aimed at probing shell-evolution have thus far focused on relatively light (A<35) isotopes [GUE09,ZEG10,MEH12], and on Gamow-Teller transitions to states at relatively low excitation energies. Fig. 2.6 shows an example for the case of Gamow-Teller transitions from the 1^+ ground state of ^{12}B to low-lying 0^+ states in ^{12}Be, mediated through the (^{7}Li,^{7}Be) reaction (in the β^+ direction) in inverse kinematics [MEH12].

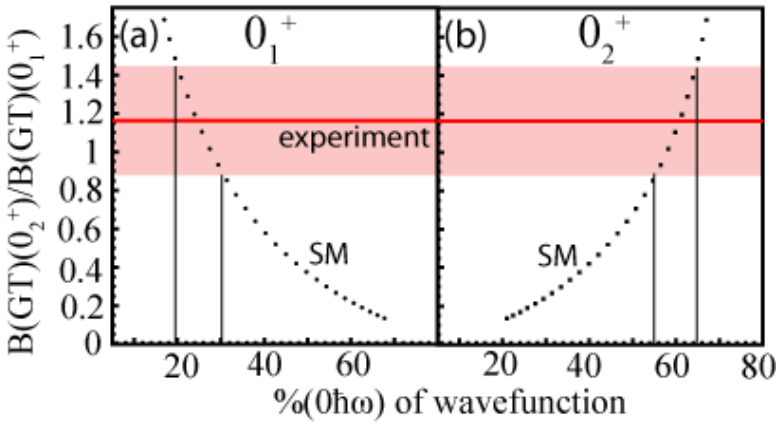

Fig. 2.6 Ratio of the Gamow-Teller strengths to the second and first 0^+ states in ^{12}Be from the ^{12}B 1^+ ground state, plotted versus the varying 0ħω content of the wave functions of the first (a) and second (b) 0^+ states produced in shell-model calculations. A large 0ħω percentage indicates a predominant p-shell nature of the wavefunction, whereas a small 0ħω percentage indicates a predominant sd-shell nature of the wavefunction of the 0^+ states. The red line with pink error band indicates the Gamow-Teller strength. ratio extracted from a ^{12}B(^{7}Li,^{7}Be)^{12}Be* charge-exchange experiment performed in inverse kinematics, which provides clear evidence for a pre-dominant sd-shell nature for the first 0^+ state, and a predominant p-shell nature for the second 0^+ state in ^{12}Be. The shell-model calculations were performed in the spsdpf model space, by making use of the WBP interaction. The figure was taken from Ref. [MEH12].

The main boundary conditions for charge-exchange experiments aimed at extracting Gamow-Teller strengths is that the beam energy should be sufficient (> ~100 MeV/u) to ensure a simple single-step direct reaction mechanism, and that cross sections are extracted at low momentum transfer (near 0^0 in the center-of-mass system) [TAD87]. Under these conditions, the cross sections are proportional to Gamow-Teller strengths (the proportionality can be calibrated by comparison to transitions for which the strengths are known from β-decay) and the strengths can be extracted model-independently with an uncertainty of about 10% for relatively strong transitions (B(GT)>0.1) [TAD87,PER11]. To separate the ΔL=0 Gamow-Teller transitions from transitions associated with larger angular momentum transfer, angular distributions must be decomposed, which requires that statistical uncertainties must be limited: rare-isotope beam intensities at the level of ~10^4-10^6 pps are required, depending on the probe studied.

With the HRS at FRIB, studies of Gamow-Teller transitions for the purpose of understanding the evolution of shell structure can be greatly expanded. Rare-isotope production rates at FRIB peak at around 170-200 MeV/u which is near ideal for ensuring a clean reaction mechanism [LOV81, OST92]. The rare-isotope production rates at FRIB and the very efficient transmission to the HRS will allow for experiments far from stability (see also Fig. 5.4). For all charge-exchange probes, the HRS would be used to detect heavy-ion reaction products. Additional detection systems are combined with the HRS for detecting recoil particles. For the (p,n) charge-exchange probe in inverse kinematics [SAS11,SAS12], the Low-Energy Neutron Detector Array (LENDA) and the Versatile Array for Neutrons at Low Energies (VANDLE) can be used to detect recoil neutrons (which are used to determine the reaction kinematics and to extract the excitation energy and center-of-mass scattering angle), in combination with the Ursinus Liquid Hydrogen target. For the (^{7}Li,^{7}Be) reaction, the Gamma-Ray Energy Tracking Array (GRETA) can be used to detect both the (stopped) 430-keV γ-ray from the first excited state in ^{7}Be (which cleanly isolates excitations associated with spin-transfer) as well as γ-rays emitted by decay-in-flight from the excited nucleus produced in the charge-exchange reaction. In addition, decay particles (neutrons and/or protons) emitted in-flight from the nucleus when excited above the particle-decay threshold can be detected in MoNA-LISA (see section 2.1) and charged-particle detectors placed after the reaction target. By employing invariant-mass spectroscopy, the excitation-energy can then be determined. Below the particle decay threshold, the excitation energy can be determined directly from the heavy-ion detected in the HRS. An alternative for the (^{7}Li,^{7}Be) reaction is the usage of the (d,^{2}He) reaction in inverse kinematics. A Time-Projection Chamber (see section 4.4) can be used to reconstruct the momentum of the unbound ^{2}He-particle from the accurate measurement of the momentum of the two decay protons. From the reconstructed ^{2}He momentum, the excitation energy and scattering angle can be determined.

2.8. Improving nuclear structure inputs to fission models

The nuclear fission process represents a very challenging and complex scientific environment with significant impact on derivative nuclear technologies in the fields of nuclear energy, defense, and homeland security. As such, the evolution of this sub-field is ongoing, with significant advances taking place on both experimental and theoretical/computational fronts.

Historically, theoretical efforts focused on the prediction of average quantities in the fission observables, or only focused on fission induced by thermal neutrons [MAD82, MOL01, BER84, GOU05]. New requirements for improved predictive capability as well as advances in computing have led to the development of more detailed models [TAL11, VOG12, BEC13]. Correlations between fission outputs and full spectral shapes are now available for experimental testing, and this more complete theoretical framework has exposed weaknesses in the understanding of nuclear structure that feeds these calculations.

Recent theoretical work has investigated the sensitivity of fission model parameters to the prompt fission γ-ray spectrum (PFGS) [TAL12,STE13a], and is complemented by next generation PFGS measurements on the major actinides [JAN13, UL14, OBS13]. The model uses a Monte-Carlo Hauser-Feshbach approach to calculate the spectrum and correlations between neutrons and γ-rays emitted from fission fragments, and the predictive capability is ultimately limited by incomplete knowledge of the nuclear structure of neutron-rich fission fragments.

In particular, experimental information regarding low-lying states in the produced fission fragments are used whenever possible, and in the continuum, a level density is assumed based on systematics. In general the fission fragments are quite neutron-rich and very little is known about them experimentally. As a result, uncertainty in how the shell structure of neutron-rich nuclei evolves ultimately manifests as systematic error in the calculation, which obscures the extraction of other model parameters such as the initial angular momentum of the fission fragments.

The broad range of intense neutron-rich beams available at FRIB could be exploited to improve the nuclear structure underpinning these calculations. In particular, γ-ray spectroscopy following fragmentation reactions at the HRS could inform these calculations directly through the measurement of discrete, low lying states. The broad momentum acceptance of the HRS, combined with the efficiency and resolution of GRETA makes surveys across large sections of the nuclear landscape between masses numbers of 80 and 140 possible.

2.9. Opportunities with commensal decay spectroscopy following reactions

In typical fragmentation or nucleon removal experiments, a large number of very exotic nuclei can be produces and transmitted to the HRS focal plane. Following particle identification detectors in the focal plane, reaction products could be implanted into an active stopper such as a Si detector array, which could act as a total kinetic energy detector, but would also be sensitive to the signals from the subsequent alpha or β decays of rare reaction products. A scintillator array immediately downstream of the implantation station would be sensitive to isomeric γ-rays, like the current S800 hodoscope, but also to delayed γ-rays following decay.

Such a focal plane detector arrangement would provide a unique opportunity to take advantage of the cocktails of rare isotopes delivered to the focal plane of the HRS in a standard experiment. These isotopes will be among the most exotic produced at FRIB, and innately of physics interest. Optimization of the HRS focal plane will allow optimal use of FRIB beams, with decay information obtained simultaneously with the (primary) physics goals of the primary experiment.

3. Direct reactions as powerful spectroscopic tools

Direct nuclear reactions have proven to be a vital tool for the spectroscopy of the single-particle components in the nuclear wave function. In a glancing collision of a projectile and a target nucleus, one or a few nucleons are transferred directly without formation of an intermediate compound system. Observables in these reactions give information about the wave function overlaps between the ground state of the projectile or target and a particular final state of the respective residual nucleus. For more than 50 years, nucleon-removing transfer reactions such as $^{A}Z(p,d)^{A-1}Z$ and $^{A}Z(d,^{3}He)^{A-1}Z-1$ have been used to probe the single-particle structure of stable target nuclei in light-ion induced transfer reactions at tandem-accelerator beam energies. However, the most exotic nuclei are usually available for experiments as fast secondary beams produced in projectile fragmentation or fission and a different approach has to be chosen to probe their single-particle structure with direct reactions.

3.1. Knockout reactions

Direct one-nucleon knockout reactions from fast exotic beams have been developed into a powerful technique, extending the detailed study of the nuclear wave function to short-lived rare isotopes [HAN03]. One-nucleon knockout reactions at intermediate beam energies have been successfully applied at rates of less than 1 particle/s. The high sensitivity is tied to the high-beam energy that (a) allows for the use of thick targets to

enable high-luminosity experiments with low beam intensities, (b) leads to strongly forward-focused reaction residues and (c) ensures an optimum signal-to-noise ratio from event-by-event particle tracking in the entrance and all exit channels [GAD08a].

In the collision of a fast projectile beam with a light, absorptive target, typically ^{9}Be or ^{12}C, a neutron or proton is removed from the projectile in a single-step, direct reaction: ^{9}Be(^{A}Z,$^{A-1}$Z+γ)X and ^{9}Be(^{A}Z,$^{A-1}$Z−1+γ)X. The shape of the longitudinal momentum distribution of the projectile-like residue carries the information on the orbital angular momentum (l-value) of the knocked-out nucleon – in analogy to the shape of angular distributions in the conventional, low-energy transfer reactions. Gamma-ray spectroscopy in coincidence with the heavy knockout residue provides the identification of the final state [GAD08a]. In comparison to reaction theory, spectroscopic factors, which relate to the occupation number of single-particle orbitals, can be derived from measured partial cross sections to individual final states of the residue. One-nucleon knockout reactions thus provide an identification of single-particle components in the ground-state wave function of the rare-isotope projectile and a measure of the relative separation and occupation of singe-particle levels. These quantities allow for the unique tracking of changes in nuclear structure beyond the valley of β-stability [HAN03,GAD08a]. The relative location of single-particle levels and their occupation by nucleons provide key benchmark tests for modern theories – for ab-initio calculations applicable for light nuclei below mass A = 12 and around doubly magic nuclei as well as for many-body shell-model approaches that are largely based on effective interactions [GRI11,GRI12].

Nucleon removal reactions have also offered a unique opportunity to probe correlation effects beyond effective-interaction theory [GAD08b]. The shell-model pictures deeply-bound states as fully occupied by nucleons. For nucleon states in the vicinity of the Fermi surface, configuration mixing leads to a gradual decrease in the associated occupation numbers. Correlations arising from short-range, soft-core, and tensor nucleon-nucleon (NN) interactions and from longer-range couplings that involve low-lying as well as giant resonance collective excitations result in a further reduction of the physical nucleon occupancies of states near the Fermi surface, the associated single-particle strength being shifted into a large number of states at higher energies [DIC03]. The occupation number is not an experimental observable but relates to the spectroscopic factor, which – in the sum-rule limit – provides the average occupancy of a single-particle orbit by nucleons. The experimental determination of spectroscopic strength thus probes the foundations of the nuclear shell model. Results of electron-induced knockout experiments suggest that single-proton states in selected stable nuclei have their occupancy reduced by factors of order 0.6–0.7 relative to independent-particle models [DIC01]. Precision (e,e'p) data illustrate quantitatively the effect of short-range correlations in terms of the depletion of the mean-field strength and the required

presence of high-momentum components in the nuclear wave function [ROH04]. The majority of (e,e'p) studies focus on closed-shell and doubly-magic nuclei and are presently limited to stable nuclei.

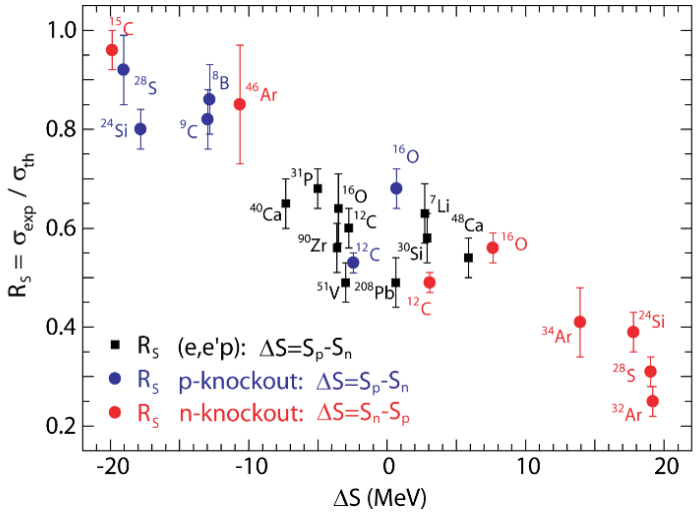

Fig. 3.1 Reduction of spectroscopic factors observed in different nucleon knockout reactions as a function of the difference in separation energies of the two nucleon species. From [GAD08b].

The Be or C-induced nucleon knockout reactions allow extending the study of spectroscopic strength to neutron single-particle states and rare isotopes (Fig. 3.1). The reduction in spectroscopic strength, $R_s = \sigma_{exp}/\sigma_{th}$, deduced from knockout experiments close to stability was found to be in agreement with the results of (e,e'p) reactions. More reduction is observed for the removal of a deeply-bound neutron from a proton-rich nucleus (the minority nucleon species is removed), while little or no reduction is observed when the majority nucleon species is knockout out (removal of a proton from a proton-rich system or the removal of a halo neutron) [GAD08b, JEN11].

The theoretical cross sections here use spectroscopic factors from configuration interaction shell model and a reaction theory description [TOS99,TOS01] in the framework of straight-line trajectories (eikonal approach) and sudden approximation. Therefore, the model dependence is reduced compared to the classical low-energy transfer reactions, whose calculation involves the Distorted Wave Born Approximation (DWBA) or higher-order formalisms, and which depend strongly on entrance- and exit-channel optical model potentials [KRA88] that have not been established for nuclei with extreme neutron-to-proton ratios. Both approximations, sudden and eikonal, become increasingly more accurate at the higher projectile energies afforded by FRIB together with the HRS. In addition, the setup of the HRS will allow measurements of the diffracted proton or neutron (the two processes in knockout are stripping and diffraction) with auxiliary detectors like

MoNA-LISA and light-charged-particle detectors in addition to the final-state identification with GRETA. This will enable the use of the reaction framework in the optimum energy regime, without kinematic limits for the removal of the most deeply-bound nucleons [FLA12], and with a direct probe of knockout mechanism via light-particle detection [BAZ09] to separate out correlation effects with reduced uncertainty on the reaction theory. For the extraction of l-values in the studies of nuclear shell structure, symmetric longitudinal momentum distributions of the knockout residues are observed at RIBF beam energy of around 200 MeV/u, see for example [KOB12], while at the lower NSCL energies of about 70-90 MeV/u, pronounced tails are encountered [GAD05]. With the increased beam energy at FRIB and the HRS, orbital angular momenta can be assigned from symmetric residue longitudinal momentum distributions unambiguously, allowing to track the evolution of nuclear structure with unprecedented clarity.

3.2. Quasifree scattering

As discussed above, knockout reactions are powerful tools for extracting information on the nuclear wavefuction. The relatively strong absorption makes the reaction probability peak at the surface of the nucleus. Similar arguments hold for transfer and Coulomb break-up reactions. To probe deeper into the nucleus, nucleon knockout reactions using protons as the probe, i.e. (p,2p) and (p,pn), have been used. Spectral functions of protons and neutrons in the wide range from valence nucleons to the deeply bound core states can be investigated. In addition, by studying cluster knockout reactions, such as (p,pd) or (p,pα), nucleon-nucleon correlations and cluster structures in nuclei can be probed. As a consequence of being deeply bound, nucleons become sensitive to in-medium modifications [KRE95], which will affect the observables measured in these quasifree reactions.

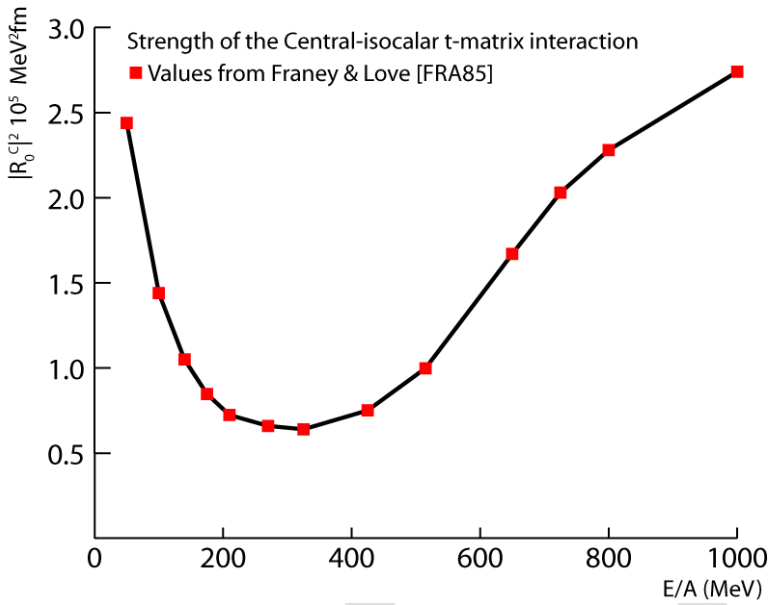

Fig. 3.2 Energy dependence of the Central-isoscalar component of the t-matrix interaction, which is responsible for distortion and final-state effects [FRA85]. For nucleon energies between 150 and 500 MeV a minimum is found and distortion and final-state interactions, which complicate quasifree knockout experiment will be minimal in this region.

The effects of final-state interactions and distortions complicate the analysis of spectroscopy experiments involving quasifree reactions. To reduce these effects it is, therefore, important to exploit quasifree reactions at beam energies where the central isoscalar component on the nucleon-nucleon interaction is minimal for both the incoming and outgoing channels (e.g. p and 2p, respectively for the (p,2p) reaction). As can be seen from Fig. 3.2, such conditions are best achieved at incoming beam energies of about 400-500 MeV/nucleon, in which case the energy of the outgoing nucleons still fall mostly in the energy region with minimum distortions (200-250 MeV per nucleon in the exit channel for equal sharing). In this energy region, it has been demonstrated that the use of a factorized impulse approximation – under the assumption that the nuclear medium does not affect the nucleon knockout process – works very well (see e.g. [HAT97]) for stable nuclei and where the knockout from deep-lying shells can be isolated from rescattering processes in the nucleus if the kinematical conditions are optimized [COW98]. The corresponding inverse-kinematics quasifree reactions program with rare isotopes is pursued at GSI/FAIR [AUM13]. This optimum projectile-beam energy regime will be opened up at FRIB following an energy upgrade to 400 MeV/u.

At FRIB, the energy of rare-isotope beams will be below the optimum regime for spectroscopic quasifree knockout studies, where distortions and in-medium effects in general play an important role (Fig. 3.2). As a result, it is not as straightforward to access and extract spectroscopic information from deeply-bound shells [FRO93,COW98].

However, if spectroscopic information is known, through Be- or C-induced knockout reactions, for example, in turn the elusive in-medium effects can be explored in the energy regime of 100 MeV for each of the two nucleons in the exit channel, providing a unique window into the role of in-medium effects in very asymmetric nuclear matter [LI93,LI94,CHE03,LI05,SAM06,JIA07], available at FRIB in form of projectile beams of the most neutron-rich nuclei.

4. Aspects of nuclear matter

One of the main goals of experiments performed at FRIB is to understand basic properties of nuclei and nuclear matter with very asymmetric neutron-to-proton ratios. It is expected that a lot of progress in understanding the nature of nuclear matter can be made by studying such asymmetric systems, as exotic features such as halos and thick neutron-skins will become prevalent for a large number of nuclei accessible at FRIB. The behavior and response of asymmetric nuclear system to external impulses has important applications beyond the realm of nuclear physics and empirical data must be analyzed in a cross disciplinary approach that involves nuclear, condensed-matter, astrophysical and atomic theory.

An example of the multifaceted approach required to make progress in key issues related to the properties of nuclear matter is the determination of the Equation-of-State (EoS). The EoS describes relationships between energy, pressure, temperature, density and isospin asymmetry (see details in section 4.4) in a nuclear system and its parameters are not only important for describing bulk properties of nuclei and nuclear matter, but also plays a key role in our efforts to describe and understand astrophysical phenomena such as neutron stars and supernovae. In particular, the isospin-asymmetric density-dependent part of the EoS has significant remaining uncertainties and a large number of experimental approaches has been used to constrain this component of the EoS. Fig. 4.1, taken from Ref. [LAT13], summarizes the current constraints obtained through various experimental approaches. Complementary studies can be found in Refs. [TSA12, HOR14].

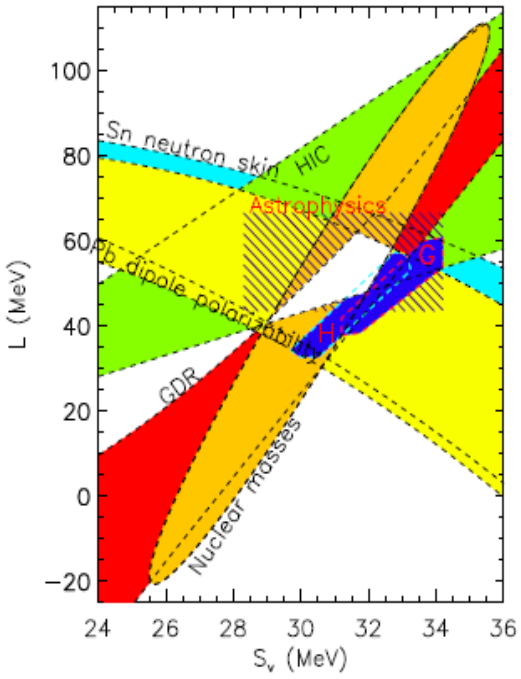

Fig. 4.1 From Ref. [LAT13] Overview of constraints provided on the symmetry energy parameters L and S_v of the Equation of State from experiments aimed at determining neutron skins, dipole polarizabilities, parameters of the Giant Dipole resonance, nuclear masses and isotope diffusion in Heavy Ion Collisions (HIC). The hatched area indicates the constraints from astrophysical observations. The enclosed white area indicates the experimentally-allowed overlap region. The two dark-blue regions labeled "H" and "G" are based on theoretical neutron matter constraints.

To make progress in studying various aspects of the EoS at FRIB, accesses is needed to the nuclei with the most extreme neutron-to-proton ratios to achieve the largest sensitivity to the relevant parameters. We also need the appropriate equipment to perform the key experiments efficiently and with good accuracy. The HRS will be critical in these efforts, as it provides the required boundary conditions and flexibility to perform a large fraction of the experiments aimed at understanding various aspects of nuclear matter as well as access to the highest rates of the most neutron-rich isotopes.

As shown in Fig. 4.1, some of the experimental constraints on the EoS are obtained from measuring the properties of giant resonances. Macroscopically, giant resonances are described as collective oscillations of the nuclear fluid that can be directly associated to the properties of nuclear matter and they can be classified as shown in Fig. 4.2 [HAR01].

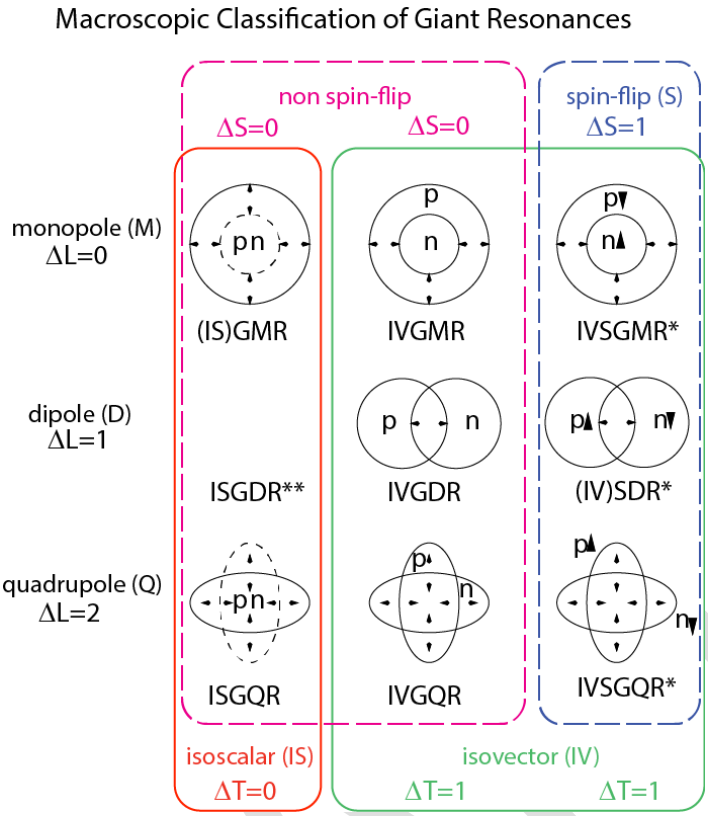

Fig. 4.2 (Adapted from Ref. [HAR01]) Macroscopic classification of giant resonances. From top to bottom: monopole (breathing mode), dipole and quadrupole excitations. Left-most column (orange): isoscalar excitations in which the proton and neutron fluids move in-phase. Two right columns (green): isovector excitations in which the neutrons and protons move out of phase. Two left columns (dashed-magenta): non-spin-flip excitations, in which nucleons with spin-up and spin-down move in phase. Right-most column (dashed-blue): spin-flip excitations in which nucleons with spin-up and spin-down move out of phase.** The Isoscalar Giant Dipole Resonance (ISGDR) is a second-order excitation and not easily depicted in this simple schematic picture. However, it has been observed experimentally [HAR01].

Microscopically, giant resonances are describes as coherent superpositions of particle-hole excitations that exhaust large fractions of so-called sumrules associated with the specific operator that describes the excitation in quantum-mechanical terms [HAR01]. These sumrules usually have simple forms and connect directly to macroscopic features, such as neutron excess or neutron-skin thickness.

Giant resonances appear at relatively high excitation energies (10-60 MeV. Several of the modes have been studied in great detail experimentally, motivated in part by the opportunties to constrain the EoS discussed above, but also to develop theoretical models based on density-functional models that are used to describe a broad range of nuclear properties, with applications in astrophysics, neutrino physics and (neutrinoless)

double beta decay. The further development and improvement of these models, and the ability to better constrain the EoS strongly benefit from experiments in which giant resonances are excited in rare isotopes, in particular very neutron-rich systems. Such experiments are challenging because the excitations occur generally far above the particle-decay thresholds: in experiments performed in inverse kinematics, it then becomes difficult to reconstruct the excitation energies, as well as other kinematical parameters which are important to characterize the reactions, such as scattering angles. In spite of such challenges, several experimental techniques have already been developed to study giant resonances in rare isotopes, which greatly benefit the design of future detection systems, in particular for experiments with the High Rigidity Spectrometer in combination with auxiliary detection systems for the detection of decay particles. In combination with the high rates of very neutron-rich rare isotopes available at the HRS, a real breakthrough in our capability to understand nuclear excitations far in the continuum can be achieved at FRIB.
In the following, several of the most important experimental approaches to study aspects of nuclear matter at the HRS are described.

4.1. Elastic scattering

The nuclear size and density distribution are important properties of nuclei that determine the nuclear potential, single-particle orbitals and wave functions. Determination of the proton and neutron densities, their rms radii (R_n and R_p) and the neutron skin thickness $S_n=R_n-R_p$ are critical for understanding the bulk properties of nuclei. The neutron-skin thickness is also closely related to the symmetry energy [BRO00, DAN03, SAG07,LAT13], which determines, for example, the radii of neutron stars [STE05]. Therefore, studies of nuclear radii are important for better understanding "the nature of neutron stars and dense nuclear matter" [LRP07]. The increased thickness of neutron skins (see Fig. 4.3) in unstable neutron-rich isotopes forms a key motivation for performing such studies at the next generation of radioactive beam facilities. Whereas charge radii can be determined by studying electron scattering, muonic atoms and laser spectroscopy via isotopic shift measurements, matter radii can be probed in nuclear reactions employing strongly interacting probes. Elastic proton scattering is one of the possible tools to perform such studies and this has already been applied to, for example, the cases of ^{4}He, ^{6}He and ^{8}He [ALK97], ^{40}Ca, ^{48}Ca [CLA03] and ^{208}Pb [KAR02,CLA03]. The main issue with such analyses is that the extraction of radii and other bulk properties is model-dependent since it relies on the comparison of theoretical calculations employing a variety of models and the data. In the case of ^{208}Pb, the first model-independent experimental information on the neutron-skin thickness has become available, namely from the parity-violating electron scattering experiment (PREX) at JLAB [ABR12] although the desired accuracy in the

neutron-skin thickness was not yet achieved. That is the goal of the follow-up experiment, PREX-II [PAS11]. In addition, a proposal for a similar experiment on ^{48}Ca has been approved [MAM13]. The JLAB data will be very valuable to constrain the theory at stability, but information on unstable nuclei, in particular with large neutron excesses, is needed to get a complete picture of the neutron-density distributions in nuclei. Systematic studies over isotopic chains extending to very neutron-rich nuclei will provide that information.

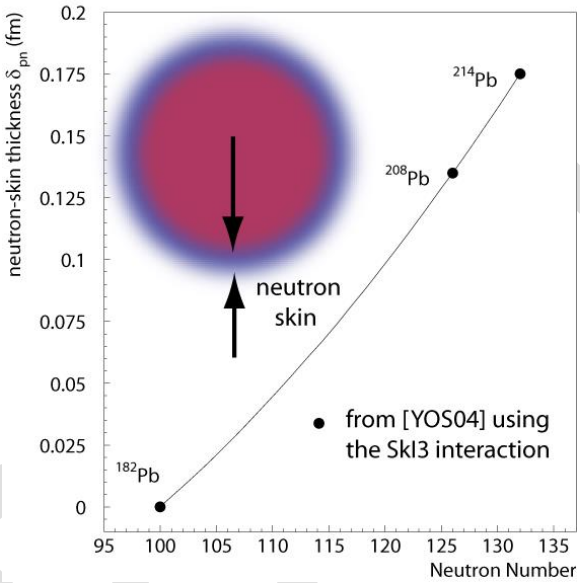

Fig. 4.3 Theoretical prediction for the change of the neutron skin thickness as a function of neutron number for Pb isotopes. The values come from Ref. [YOS04] using the SKI3 interaction. The line is drawn to guide the eye.

The key to ensuring that proton elastic scattering data provide accurate information on density distributions and matter radii is to confirm that the extracted parameters are beam-energy independent [CLA03,KAR02]. This can be done by analyzing the elastic differential cross section within a consistent theoretical framework over a wide range of momentum transfers (i.e. up to large scattering angles) for a variety of beam energies. Consistent results at different beam energies would provide a strong indication that the nuclear structure part of the analysis is well integrated with the reaction theory and that necessary theoretical approximations are appropriate. Such studies over quite a broad range of beam energies can be performed at the next generation of rare-isotope beam facilities, and FRIB will be able to push out furthest towards the most neutron-rich isotopes. In order to provide stringent constraints on the theory, relatively high statistics data for elastic scattering must be acquired. To do so effectively over a large momentum transfer

range and for a chain of isotopes, the use of a thick Hydrogen target is strongly preferred. Precise information on momenta and scattering angles are equally crucial. At the HRS, such experiments can be performed most efficiently. For example, experiments along the chain of Calcium isotopes can be achieved up to A=56 (predicted rate of ~200 pps at a magnetic rigidity of 6 Tm).

4.2. Total reaction/interaction measurements

Absorption measurements are complementary to elastic proton scattering. They can also provide information about the matter radii of isotopes [OZA01]. Such experiment can be divided into two classes: (i) reaction cross section (σ_R) measurements, in which the total probability of interaction between a nucleus and a target is determined from a measurement of the particles transmitted through a target without any interaction and (ii) interaction cross section (σ_I) measurements, in which the total probability of a reaction between a nucleus and a target is measured for which the nucleus changed proton and/or neutron number. The difference between σ_R and σ_I are inelastic-scattering events, i.e. events in which energy and momentum is transferred between nucleus and target but the neutron and/or proton number does not change: $\sigma_R=\sigma_I+\sigma_{inelastic}$.

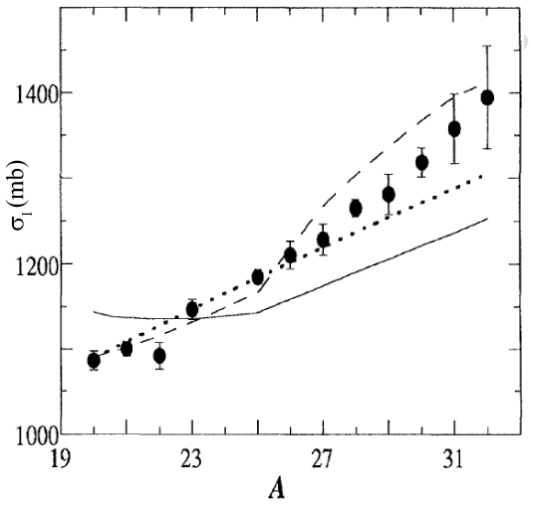

Fig. 4.4 Measured Interaction cross sections for Na isotopes on carbon targets at 950 AMeV [SUZ95]. The lines correspond to a simple mass-dependent approximation (dotted), a Glauber calculation (solid) and a relativistic mean field calculation (dashed).

Similar to the case of elastic proton scattering experiments, the main problem lies in the interpretation of the measured cross section in terms of density distributions and matter radii. The analyses are model dependent and usually a Glauber model in the optical limit is used, which has been shown to work reasonably well at higher beam energies for stable

nuclei (400-800 AMeV) (see [OZA01] and references therein). For loosely bound systems, corrections to such models are probably necessary [ALK96], although a model-independent-method to test the validity of the theoretical approaches is still lacking. Because of the additional assumptions made on the inelastic scattering cross section when using the interaction cross section for the determination of matter radii, the use of the reaction cross section is in principle preferable. However, measurements of σ_I are easier than those of σ_R since no distinction has to be made between inelastic and elastic scattering. Measuring the momenta of transmitted particles with sufficient resolution to separate elastic and inelastic reactions can only make the latter distinction. In spite of such uncertainties, positive result have been reported, e.g. for He isotopes [TAN92] and Na isotopes [SUZ95] (see Fig. 4.4).

Amos et al. [AMO06] studied the prospect of studying the reaction cross sections on protons as a tool to measure the spatial distribution of neutrons in exotic nuclei [AMO06] and they showed that by folding nuclear structure functions with effective in-medium nucleon-nucleon cross interactions good descriptions of the reaction cross section data can be achieved at energies from 65-200 AMeV. As before, the analysis is model-dependent, but this result opens new opportunities for studying reaction cross sections at FRIB. And at such energies, separation between inelastic and elastic channels is feasible even for relatively massive nuclei) if a spectrometer with the optimum properties is used. With the HRS, studies can be performed over a wide beam-energy range, which will help to constrain the systematic uncertainties. In addition, being able to achieve the highest rare-isotope beam intensities for the most neutron-rich nuclei is of course critical and will be achieved at the HRS.

4.3. Heavy-ion electromagnetic excitations

Electromagnetic excitations induced by heavy ions (Coulomb excitation) at intermediate and relativistic beam energies have long been used to provide detailed information about collective degrees of freedom in nuclei [BER88,GLA98]. Excitations of rare isotopes can be studied by scattering these particles of a stable high-Z target; the exchange of virtual photons, when the rare-isotope beam passes through the Coulomb field of the high-Z target, results in high cross sections for collective excitations. By selecting events in which the projectile is scattered at very forward angles (i.e. at large impact parameters), the electromagnetic process dominates over the nuclear interactions mediated by the strong force.

For a given secondary beam and target, the sensitivity for exciting a particular collective state strongly depends on the choice of the beam energy. This is illustrated in Fig. 4.5, which shows the dependence of the Coulomb cross section as a function of beam energy for different collective excitation modes [GLA98]. The first excited 2^+ state is most

strongly excited at low beam energies, and the excitation probability of the higher-lying Giant Dipole Resonance (GDR) and Giant Quadrupole Resonance (GQR) increases steeply at higher beam energies.

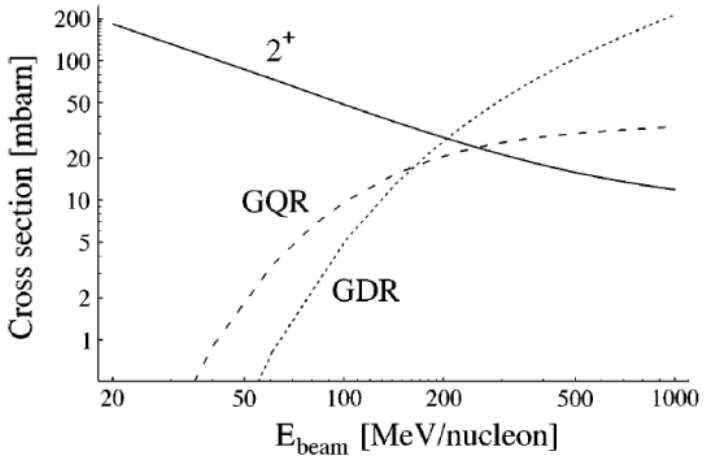

Fig. 4.5 Energy dependence of the Coulomb excitation cross section of the first excited 2^+ state, the giant dipole resonance (GDR) and the giant quadrupole resonance (GQR). From [GLA98]

Experimental studies at both intermediate (~100 AMeV) and relativistic (~ 1 AGeV) beam energies have already been employed with great success. At the intermediate energies, chains of isotopes can be studied simultaneously, providing a consistent set of measurements while minimizing systematic uncertainties. Measurements of the scattered projectile are performed in coincidence with the de-excitation photons tagging the inelastic process. Both the location of the excited state, as well as the cross sections from which $B(\Sigma\lambda)$ transition strengths can be deduced provide stringent tests for theory since the evolution of collectivity can be probed as a function of neutron number (see e.g. Ref. [YUR04] for the case of Ni-isotopes). Such studies will certainly be an important component of the future program at FRIB and can be performed at the HRS in combination with GRETA. Even though it is preferable to run at somewhat lower beam energies (lower magnetic rigidities) to study the first 2^+ state, the excellent transmission efficiency from the fragment separator to the HRS will be very helpful for performing experiments with the most neutron-rich nuclei that are produced at the highest yields at magnetic rigidities beyond the capability of the S800 spectrograph and the analysis beam-line system.

To efficiently study the GDR and GQR at FRIB, experiments should be performed close to the beam energies at which the production rates are maximum (170-200 MeV/u). Especially the excitation of the Giant Dipole Resonance is of great interest, since its properties provide a probe of charge distributions in nuclei. A fragmentation and a shift of the GDR strength towards lower excitation energies was predicted for heavier nuclei

as the neutron dripline is approached [SUZ90]. This redistribution of strength is due to changes in the nuclear mean field as a function of N/Z ratio combined with the proximity of the continuum for all particle-hole excitations [ZEL06]. Such a redistribution of strength towards lower energies was, for example, observed in studies of the GDR in ^{130,132}Sn [ADR05]. Studies of the existence and low-lying dipole strength in neutron-rich nuclei is not only of importance for understanding collective motions in asymmetric nuclei, it is also important for relative abundances produced in the astrophysical r-process [SAV13]. Although during much of the r-process, photodisintegration and radiative capture are in equilibrium, near the end of the process, nucleosynthesis depends on the absolute rates of the (n,γ) and (γ,n) processes and the latter will be affected by the low-lying dipole strength. For example, in the region near the above-mentioned cases of ^{130,132}Sn, several waiting points in the r-process path are nearby and could be affected. Therefore, studies of the GDR have important implications for astrophysics (see also section 5).

Measurements such as the one performed by Adrich et al. [ADR05], require several detector systems. Since the main component of the dipole strength is situated above the particle separation threshold, the excited nuclei will break up in flight. To reconstruct the excitation energy spectrum, the momenta of the neutron(s) emerging after projectile dissociation must be measured, photons from the decay must be detected and the momentum of the residual must be determined. A combination of the HRS, MoNA-LISA and efficient photon detection using GRETA would be ideally suited for such experiments.

4.4. Equation-of-State studies using heavy-ion collisions

At low temperature, the EoS can be separated into a symmetric matter contribution that is independent of the isospin asymmetry and a poorly constrained symmetry energy term, proportional to the square of the asymmetry [LI08, LAT01, LAT04]. Uncertainties in quantities such as the three-body neutron force contribute significantly to uncertainties in the density dependence of the symmetry energy [HEB10, GAN12]. An improved understanding of the symmetry energy will improve predictions for masses [DAN03], fission barriers, energies of collective vibrations [LI07, DAN03] and E1 strength [CAR10, TAM11], and the thickness of the neutron skins of neutron-rich nuclei [BRO00, HOR01].

Macroscopic quantities of asymmetric nuclear matter exist in neutron stars and in type II supernovae over a wide range of densities [LAT01]. Constraints on the EoS and the symmetry energy at sub-saturation and supra-saturation densities can improve our understanding of neutron-star properties such as stellar radii and moments of inertia, crustal vibration frequencies [LAT04,VIL04], and neutron-star cooling rates [LAT04,STE05] that have been investigated with ground-based and satellite observatories. Consequently, the goal of determining the EoS has been a major motivation for recent analyses of X-ray observations aimed at extracting the correlation between neutron-star

masses and radii [STE10, SUL11, GUI13]. These analyses of neutron-star observations currently lead to strongly divergent conclusions about the EoS of neutron-rich matter at approximately twice saturation density [HOR14].

The EoS of cold nuclear matter can be written as the sum of the energy per nucleon of symmetric matter and a symmetry energy term [LI08],

$$E(\rho, \delta) = E_0(\rho, \delta=0) + S(\rho)\delta^2, \qquad (1)$$

where the asymmetry $\delta = (\rho_n - \rho_p)/\rho$, and ρ_n, ρ_p and ρ are the neutron, proton and nucleon densities, and $S(\rho)$ describes the density dependence of the symmetry energy. Measurements of isoscalar collective vibrations, collective flow and kaon production in energetic nucleus-nucleus collisions have constrained the EoS for symmetric matter, $E_0(\rho, \delta=0)$, at densities ranging from saturation density to five times saturation density [DAN02, FUC06, YOU97]. The extrapolation of the EoS to neutron–rich matter depends on $S(\rho)$, which has had few experimental constraints [BRO00] until recently.

Laboratory constraints are now emerging from experimental data especially at sub-saturation densities [TSA12, LAT13, HOR14], see also Fig. 4.1. A set of constraints on the symmetry energy as a function of density from experimental measurements are shown in Fig. 4.6. At sub-saturation densities ($\rho/\rho_0 < 1$), the constraints from heavy-ion collisions [TSA09], isobaric analog states (IAS) [DAN13], and nuclear masses of neutron-rich nuclei [ZHA13, BRO13] are reasonably consistent. This agreement bodes well for the use of heavy-ion collisions as a probe of the symmetry energy above saturation density where the current constraints are inconsistent [XIA08, RUS11], as shown in Figure 4.6.

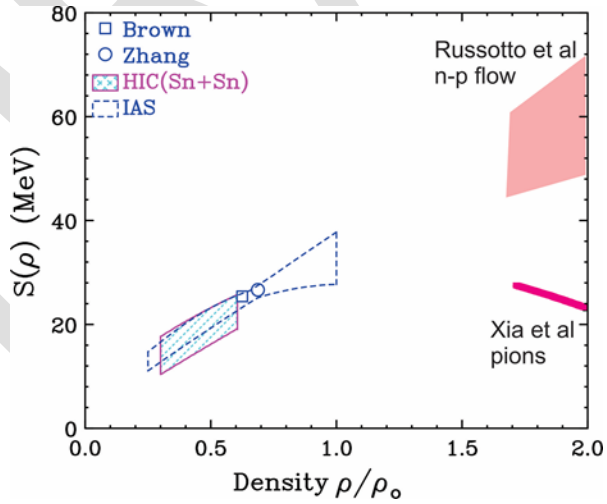

Fig. 4.6 Constraints on the symmetry energy, S(ρ), as a function of density. The constraints are discussed in the text.

While many nuclear structure and reaction observables can constrain the EoS for neutron-rich matter at sub-saturation densities, experimental constraints at supra-

saturation densities, where the uncertainties are greatest, can only be provided by measurements of nucleus-nucleus collisions. The symmetry energy at high-densities can be probed from heavy-ion collisions by comparing the relative emission of members of isospin multiplets, e.g. π^- vs. π^+, *n vs. p, t vs.* ^{3}*He, etc*., which experience symmetry potentials and symmetry forces of opposite sign [FAM06, LI05, LI05b, ZHA14,COU12,DIT10, XIA08, BAR01, HON13]. Furthermore, it was recently shown that measurements of the <N/Z> of projectile-like fragments from heavy-ion collisions can provide another link to the symmetry energy [KOH13]. These measurements should probe the sub-saturation density region. Thus, the ideal experiment would provide simultaneous measurements of pions, neutrons/protons, light charged particles, and projectile-like fragments from heavy-ion collisions induced with neutron- and proton-rich radioactive ion beams (RIBs). FRIB will provide these RIBs at maximum intensity at energies of 170-200 MeV/u which will allow for studies of the symmetry energy at both sub- and supra-saturation density.

Significant constraints on the density dependence of the symmetry energy can be enabled by installing a Time Projection Chamber (HRTPC-AT) in front of the HRS at FRIB. The HRTPC-AT would allow two operating modes: 1) a conventional TPC with an internal fixed target and 2) an active target. The design of this TPC would be optimized for coincidence studies between charged particles and pions detected in the TPC, neutrons detected in MoNA-LISA, and heavy ions detected in the HRS. This combination of detection capabilities would allow for a diverse experimental approach for studying the density dependence of the symmetry energy.

In internal target mode, the HRTCP-AT would enable:

1. Comparisons of π^- and π^+ spectra and flows in collisions with the most neutron-rich and neutron-deficient systems such as ^{136}Sn+^{124}Sn and ^{106}Sn+^{112}Sn. Calculations predict that this would provide constraints on the symmetry energy at $1.5\rho_0$.
2. Comparisons of t and ^{3}He spectra and flows in collisions with the same systems. In addition to enabling constraints on the symmetry energy at $1.5\rho_0$, this allows constraints on the momentum dependence of the symmetry energy, and on the difference between the neutron and proton effective masses.
3. Experimental probes of the neutrino-sphere Equation of State. This involves using the HRTPC-AT as a centrality trigger and charged particle detector in combination with external charged particle and neutron detectors and an external high resolution recoil separator, such as the High Rigidity Spectrometer. This provides high-resolution measurements, under laboratory controlled conditions, of neutron-rich matter at neutrino-sphere densities.

In active target mode, the HRTPC-AT would enable measurements of inelastic and charge-exchange reactions used for studying isoscalar and isovector giant resonances

(see section 2.7), as well as Gamow-Teller strength distributions for astrophysical purposes (see section 5.3).

4.5. Isoscalar giant resonances

The energy of the isoscalar giant monopole resonance (ISGMR) or the nuclear "breathing mode" is directly related to the nuclear incompressibility, a critical component of the nuclear equation of state. In recent years, measurements of ISGMR over series of Sn and Cd isotopes [LI07,PAT12] have provided an "experimental" value for the asymmetry term of nuclear incompressibility, K_τ (K_τ = -550 ± 100 MeV); this term is governed by the first and second derivatives (as a function of density) of the symmetry energy at sub-saturation densities [COL14] and, as discussed above, is important in the studies of, among other things, neutron stars. Extending these measurements to very neutron-rich isotopes is very important to more precisely determine the value of this asymmetry term. Another important issue that would be addressed by ISGMR measurements in very neutron-rich nuclei is that of the "soft" monopole resonance resulting from the vibrations of the neutron skin; one would then have an incompressibility of the core and another one of the skin. This would result in ISGMR strengths at low energies—the "pygmy" monopole resonance akin to the pygmy dipole resonances observed in many nuclei [SAV13].

A first measurement [MOR08] of the ISGMR in an unstable nucleus (^{56}Ni) was performed by injecting the rare-isotope beam into an active target TPC filled with deuterium gas. From the measurement of the recoiling deuteron in the (d,d') reaction the kinematical observables could be determined and the excitation energy and scattering angle derived. Very recently [VAN14], a successful measurement of the ISGMR in ^{68}Ni was reported, based on a similar technique, but employing (α,α') scattering by filling the TPC with Helium gas. In this experiment, first indications for the soft component of the ISGMR were observed.

At FRIB, experiments aimed at extracting the ISGMR can be performed with very neutron-rich and very neutron-deficient nuclei by placing the HRTPC (see also section 4.4) in front of the HRS. The HRTPC would be used to detect the recoil particle (either the deuteron or α-particle) and the HRS would detect the heavy nucleus to provide a clean trigger. For example, the ISGMR could be studies in Sn isotopes with mass numbers ranging from 104 to 134 for which intensities of ~10^4 pps are available with the excellent transmission from the FRIB fragment separator to the HRS. Such measurements would reduce the uncertainty in K_τ by more than a factor of 2 (see Fig. 4.7). The measurement in which the HRTPC is placed in front of the HRS can also be expanded by measuring decay particles (neutrons in MoNA-LISA and protons/light charged particles in a charged-particle array placed at the exit of the HRS) from the excited nucleus to further constrain and better reconstruct the reaction.

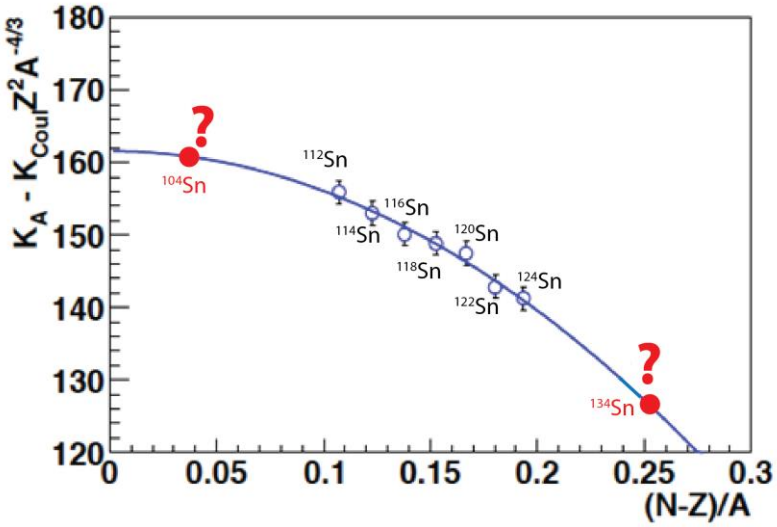

Fig. 4.7 Systematics of the nuclear incompressibility, K_A (minus the Coulomb term), derived from measurement of the ISGMR in Sn isotopes, as a function of the asymmetry term (N-Z)/A. The data are from [LI07]; also shown is a quadratic fit to the data leading to a value for the asymmetry term of nuclear incompressibility K_τ = -550 ± 100 MeV. A measurement of the ISGMR in ^{104}Sn and ^{134}Sn to within ±0.2 MeV would reduce the uncertainty in K_τ to less than 50 MeV.

4.6. Isovector giant resonances

As shown in Fig. 4.2, isovector giant resonances are associated with out-of-phase density oscillations of the proton and neutron fluids in nuclei [HAR01]. Their study, through charge-exchange reactions at intermediate energies, provides thus access to macroscopic nuclear matter properties associated with the difference between the two fluid components such as the symmetry potential and the neutron-skin thickness [DAN03]. By varying the neutron-to-proton ratio in probed nuclei, preferably along an isotopic chain, sensitivity is gained to these properties. Another degree of freedom arises from spin oscillations of the nucleons, leading to the isovector spin-flip giant resonances. The study of these resonances are therefore also excellent probes of isovector spin-isospin sector of the nucleon-nucleon effective interaction [FRA05] and are desirable for improving the reliability of shell-model, mean-field or other density-functional calculations (such as the quasi-particle random-phase approximation (QRPA)) [LIT14], which have many applications, including the description of astrophysical phenomena [LAN03] (see section 5.3) and neutrino-less double β-decay (see e.g. [ELL02,EJI05]).

The two simplest isovector giant resonances are the Isobaric Analog State (IAS) and the Gamow-Teller Resonance. The IAS and GTR have been well-studied in charge-exchange reactions, and because their structures are relatively simple, used to gain information

about the properties of nuclear matter. For example, the energy splitting between the IAS and the centroid of the Gamow-Teller resonance provides a measure of the neutron-skin thickness [VRE03]. More recently [LOC14], the extraction of the neutron-skin thickness through the analysis of the differential cross section for the excitation of the IAS was shown to produce results consistent with other approaches.

Another method used to extract information about the neutron-skin thickness, is by extracting the sumrule value for the isovector spin-dipole resonance (IVSDR), which is directly related to the thickness of the neutron skin [HAR01]. Two sets of experimental studies have been performed on stable nuclei [KRA99, YAK06]. The sensitivity of these experimental approaches involving isovector giant resonances to constrain the thickness of the neutron skin suffer from systematic errors that are comparable in size to the signal. A fruitful approach is to perform a consistent analysis along a chain of isotopes [KRA99] so that systematic uncertainties are largely common and cancel, and to perform experiments with large signal (neutron-skin thicknesses), which requires performing experiments far from stability. Fortunately, the cross sections for the relevant giant resonances are relatively large and are readily identified in experimental data, making them very suitable for investigations involving rare isotopes, where the neutron skins become thick and the sensitivity of the experimental signal much stronger [SAG07]. In addition, constraints on the isovector spin-isospin components of the nucleon-nucleon interaction will be much more stringent, if data can be collected on unstable, very proton-neutron asymmetric systems.

The energies for which the rare isotope yields produced at FRIB are maximum (~170-200 MeV/u) are ideal for studies of the isovector spin-isospin excitations and allow for studies far from the valley of stability. Distortions by the nuclear mean-field that complicate the reaction mechanism are minimal at ~200 MeV/u reducing the uncertainties in the extraction of transition strengths associated with the excitation of the isovector giant resonances [LOV81,OST92].

To achieve the scientific goals of characterizing isovector giant resonances in unstable nuclei, the use of the HRS and auxiliary detection systems are critical and the techniques for performing these experiments have already been described in section 2.7.

A separate, but also very interesting prospect is to use rare-isotope beams as probes to isolate specific spin-isospin responses, including those of giant resonances. For example, In the past few years, the (^{10}C,^{10}B+γ) [SAS12a] and (^{10}Be,^{10}B+γ) [SCO14] probes have been developed at RIBF and NSCL to seek for unambiguous evidence for the elusive isovector giant monopole resonance [HAR01] (IVGMR, see also Fig. 4.2), which is the isovector partner of the isoscalar giant monopole resonance. A detailed knowledge of its properties will complement information about the equation of state of nuclear matter obtained from the properties of the ISGMR [HAR01] and further constrain the EoS.

Because the IVGMR is not associated with spin transfer ($\Delta S=0$), it is very difficult to isolate its signature in charge-exchange experiments with usual probes, since spin-transfer transitions ($\Delta S=1$) strongly dominate at intermediate energies [LOV81]. Previous studies suffered from large and poorly understood backgrounds [ERE86,IRO86,NAK99].

By impinging unstable ^{10}C or ^{10}Be (both have $J^{\pi}=0+$) beams on stable targets, and gating on γ-rays from the 0^{+} excited state in ^{10}B (1.022 MeV γ-ray from the decay of the 1.74 MeV 0+ state) that are produced in-flight, a clean $\Delta S=0$ filter can be created. For the (^{10}Be,^{10}B+γ) experiment [SCO14] GRETINA was used to detect the 1.022 MeV in-flight γ-ray. A combination of the HRS with GRETA would create the ideal environment to perform experiments with rare isotope probes that isolate specific modes through γ-ray tagging. Whereas at present, measurements are restricted to the study of relatively light nuclei (in the (^{10}Be,^{10}B+γ) experiment, ^{28}Si was studied) because cross sections drop rapidly with increasing mass number due to distortion effects, with the combination of the HRS and GRETA, exotic giant resonances in heavy nuclei can be closely examined. It should be noted that these experiments are performed in forward kinematics, and to achieve reasonable excitation energy resolution, the beam line towards the HRS should be operated in dispersion matched mode.

5. Nuclear astrophysics

Nuclear astrophysics is a dynamic field in which information from multiple disciplines must be combined to answer fundamental questions about our universe. Astronomical observers and modellers, experimentalists and theorists work hand in hand to solve fundamental nuclear astrophysics questions: What are the origin of the universe? What is the nature of dense and exotic astronomical phenomena, such as neutron stars? How do stars evolve and explode? These and more detailed subquestions are summarized in the Nuclear Astrophysics Whitepaper [AST14]. It is clear that information about nuclear physics processes (summarized in Fig. 5.1) are key to solving these questions. However, in spite of a significant amount of information that has been gathered over many decades, answers to these questions are still incomplete in many aspects. For example, for the r-process, which is responsible for the creation of many of the elements heavier than iron, and the p-process, which is responsible for the creation of about 30 proton-rich elements, the astrophysical sites have not been determined.

Although major improvements to the facilities and equipment available for measuring nuclear physics data of importance for nuclear astrophysics have been made over many years, a major hurdle has been the limited ability to perform measurements on nuclei that are far from stability but that play major roles in the astrophysical processes shown in Fig. 5.1. FRIB provides a huge opportunity to make inroads into this "terra incognita" of the nuclear chart which is so important for solving the above-mentioned questions. The High-

Rigidity Spectrometer will be critical to the efforts at FRIB related to nuclear astrophysics, since it is designed to perform experiments with beams at energies at which the production rate is maximal with very limited losses in beam transportation to the spectrometer, allowing for access to very neutron-rich isotopes including a significant fraction of those in the r-process path (see Fig. 1.1).

The nuclear physics data needed for astrophysical purposes is very diverse. For many processes information about a particular property or reaction on (sets of) specific isotopes are required. For other purposes it is very important to ensure that the theoretical models that are being used to estimate specific properties of nuclei or reactions are reliable and the uncertainties are quantifiable since these properties or reactions are not measurable under terrestrial conditions. Therefore, experiments at the HRS aimed at providing a description of nuclei and nuclear matter as described in sections 2 and 4 have major impacts on the ability to understand and describe astrophysical phenomena. A clear example is the effort, through various experimental techniques, to constrain the equation of state of nuclear matter, which is of direct importance for understanding hot and/or dense astronomical objects, such as supernovae and neutron stars, as described in section 4. Efforts aimed at understanding the evolution of nuclear structure far from stability have great direct impact (e.g. by reducing or completely removing the need to extrapolate nuclear models to very asymmetric regions of the chart of nuclei) and indirect impact (e.g. by pinning down the modifications to the nuclear potential and improving the quality of the nucleon-nucleon interaction used in theoretical models). In addition the motivations for experiments with the HRS at FRIB described in sections 2 and 4, this section describes several other important types of experiments with strong astrophysical motivations.

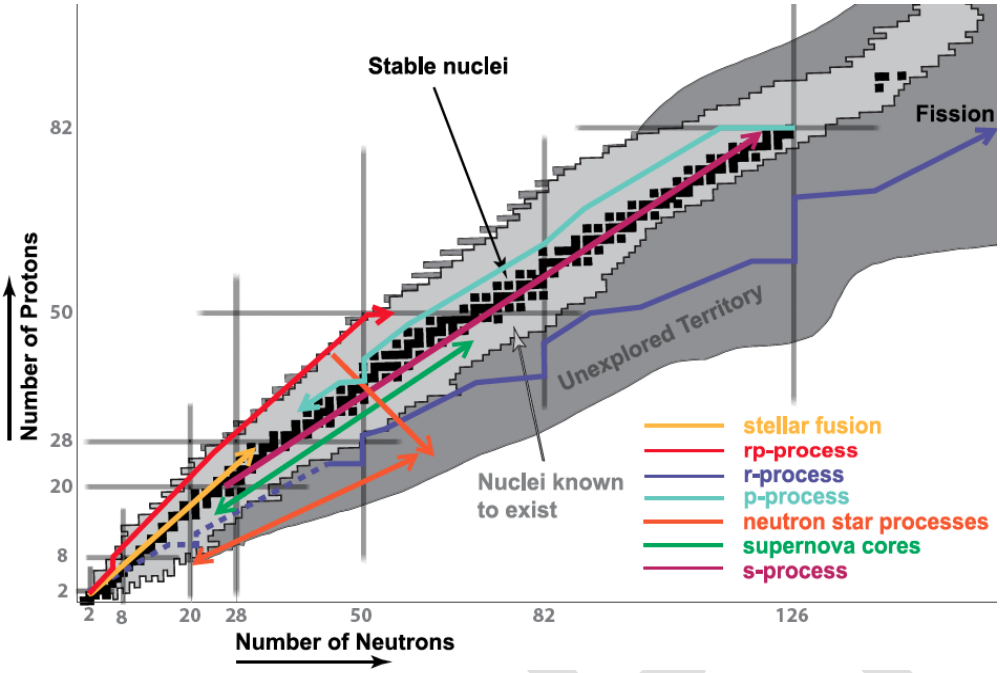

Fig. 5.1 Overview of the main astrophysical processes superimposed on the chart of nuclei (Figure from F. Timmes)

5.1. Time-of-flight mass measurements

Nuclear mass excesses reflect nuclear binding energies and provide a global view of the nuclear landscape. Shell closure, deformation and pairing have clear signatures in the nuclear mass surface. Nuclear mass-excess data are essential for predictions of the limits of stability, the nuclear synthesis paths in supernovae and neutron star mergers, and neutron star crusts. Predictions from nuclear mass models [ERL12] agree quite well for nuclei for which the masses have been measured, but the divergence between different model predictions grow steadily (to several MeVs) when extrapolating into the regions where data are not available, in particular on the neutron-rich side. The primary reason for the discrepancies between the different models is the uncertainty in the dependence of the nuclear forces on neutron excess and mass measurements contribute strongly to constraining these forces. For astrophysical purposes, the uncertainties are much larger than acceptable for applications in astrophysical modelling, and it is very important to improve the inputs. As a general rule, measurement of mass excesses of nuclei far from stability with a precision of 0.1-0.5 MeV are required. Data on a large number of nuclei are needed to reveal systematic trends in the mass surface that have a particularly strong impact on astrophysics and on nuclear structure conclusions. Such data can be provided through Time-of-Flight magnetic rigidity (ToF-Bρ) mass measurements. Such measurements are complementary to high-precision mass measurements that can be

performed for a smaller group of key nuclei through measurements in Penning traps, and more recently with multi-reflection time-of-flight devices. The ToF- Bρ method has a lower precision than these methods but can provide data several neutron units further from stability, especially for short-lived isotopes [EST11,GAU12,MEI13]. In addition, with the ToF-Bρ method, data on a large number of nuclei can be obtained in a single experiment. The potential of such measurements at FRIB is illustrated by Fig. 5.2 [MEI13]. In which the region in the chart of nuclei for which the rare-isotope beam intensity exceeds 10^3 particles/day (~0.01 particles/s), which is, at present, a reasonable rate needed to reduce statistical uncertainties of the measurements to the desired levels. This region covers the full r-process path up to neutron number N=100 and approaches the r-process path up to N=140. It also covers a significant fraction of the neutron-rich nuclei of importance for processes in the crusts of neutron stars.

The HRS provides an excellent environment to perform ToF- Bρ measurements. The total combined length of the beam line and the spectrometer is about 65 m and the approximate time-of-flight of the isotopes at the energy for which the rate is maximized (170-200 MeV/u) is about 400 ns. Compared to recent ToF-Bρ measurements, it will be possible to improve the resolution of the position and timing measurements to about 0.1 mm and 5 ps (LAP14). With those resolutions, a mass-excess measurement with a precision of 0.2 MeV in the mass A=100 region can be achieved at the HRS. In addition, the improved resolutions will help reduce systematic errors in the measurements. In summary, the ToF-Bρ measurements at the HRS provide an excellent way to complement mass measurements through other techniques, in particular for the region in the chart of nuclei that are furthest from stability and that will have the highest impact on nuclear astrophysics.

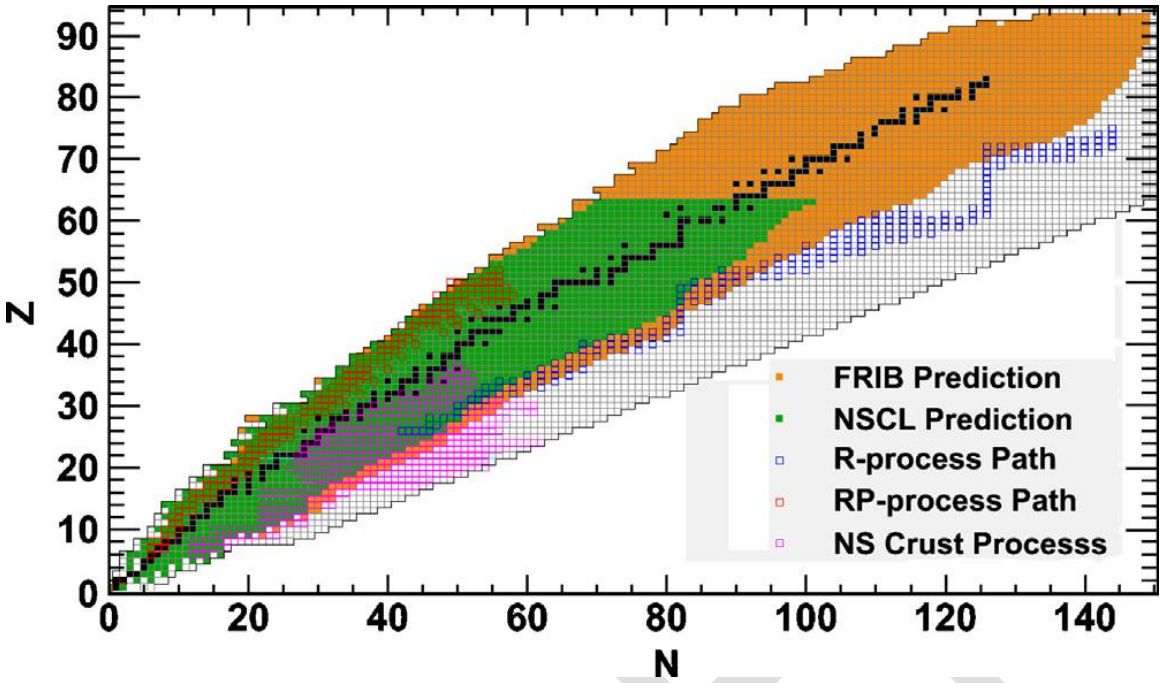

Fig. 5.2: Nuclei with predicted rates >1000/day at the NSCL (green) and at FRIB (brown) [MEI13]. At FRIB, a large fraction of the nuclei in the r-process path (blue) up to A~100 can be covered and up to A~140 closely approached. A significant fraction of the nuclei of importance for neutron-star crustal processes (up to A~60) can also be measured at the HRS using the ToF-Bρ technique.

5.2. Projectile fragmentation and in-flight fission of neutron-rich nuclei

Fission properties of neutron-rich isotopes are an important input for astrophysical models of nucleosynthesis during the r-process. As the sequence of neutron captures and β decays that drives the r-process takes the matter flow towards very heavy isotopes, different fission modes (spontaneous, induced and β-delayed fission) will become the dominant reaction types [PAN04] and responsible for the end-point for the r-process. Therefore, fission halts the reaction flow to the heavier masses and determines how heavy the elements that can be synthesized by astrophysical processes are. Fission can also affect the final abundances of the produced heavy elements. For example, when nuclei decay towards stability at the end of the neutron-capture stage, β-delayed fission will reduce the amount of cosmochronometer isotopes, such as Uranium and Thorium, that are synthesized in the r-process [THI83, SCH02]. Fission processes also have an important global effect on the abundance patterns of r-process isotopes in the mass region of fission fragments. Reliable data on the isotopic distribution of fission fragments is necessary to understand this effect, in particular in proposed r-process scenarios at sites with very high

neutron density, such as that present in the merger of binary neutron-star systems. In such scenarios the reaction flow will go through several cycles of synthesis up to heavy masses, followed by fission-recycling back to intermediate mass region [KOR12, GOR13]. The distribution of fission fragments then leaves a strong imprint on the resulting r-process abundances, and can contribute to a robust abundance pattern of individual r-process events. For example, in the model of Goriely et al. [GOR13], the production of the rare-earth peak, one of the salient features of r-process abundance patterns, is formed as direct consequence of fission fragments from isotopes in the end point of the r-process, as shown in Fig. 5.3. The result of Ref. [GOR13] illustrates the need for new experimental information on fission fragment distribution in neutron-rich isotopes: their fission model predicts a double-asymmetric fission mode for the A=278 isotones (main progenitors of the rare-earth peak in their r-process calculation) that has never been observed experimentally.

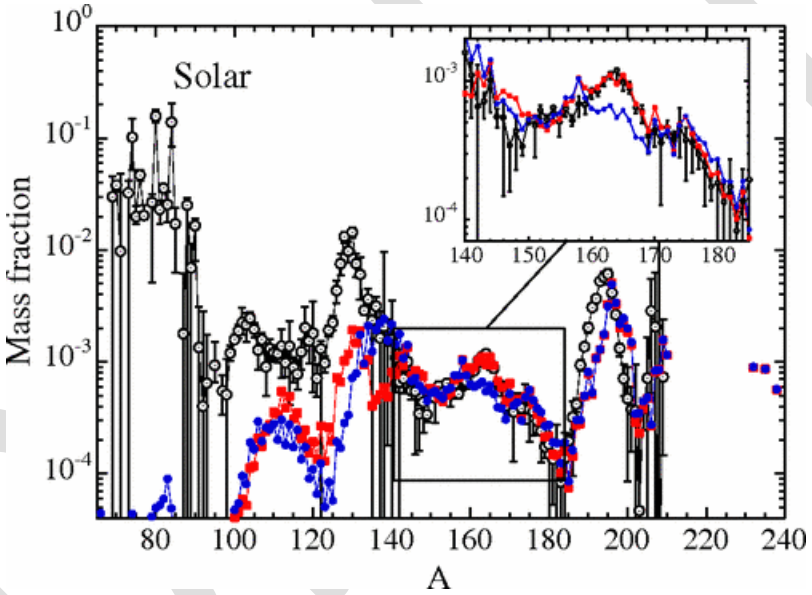

Fig. 5.3 (from Ref. [GOR13]) Final abundance distributions for ejecta produced in neutron-star (of 1.35 solar masses) mergers. The blue and red dots represent results based on different models for the fission process. The open circles represent solar abundances.

The renewed interest on fission data for the r-process has resulted in several recent theoretical calculations of fission properties of neutron-rich nuclei (e.g. [GOR13, ERL12, MOE09]). These are very challenging calculations, which require, for example, multidimensional minimizations of the energy of the two nascent fragments as a function of deformation and the considerations made for the structure of the nuclei involved. Experimental data on the neutron-rich side to constrain and validate these theories is lacking. Steady progress on fission measurements on the proton-rich side show the

potential of having appropriate data to improve our understanding of the fission process, for example with the discovery of new types of asymmetric fission in proton-rich mercury isotopes [AND10]. The measurement of fission fragment distributions with experiments in inverse kinematics has been proved to be a powerful technique that can achieve very good resolution ([SCH01, CAA13, PEL13]). The ability to produce very neutron-rich heavy beams at FRIB, coupled with the excellent transmission to the HRS, allows for detailed measurements of fission-fragment distributions in unexplored regions of the nuclear chart, thereby providing critical data for r-process calculations as well as a better understanding of the physics of nuclear fission.

5.3. Weak reaction rates for astrophysics

Understanding the evolution of supernovae is critical for our understanding of the universe. Not only are supernovae sites for nucleosynthesis, their shockwaves are thought to be major drivers for galactical chemical evolution. In spite of their important roles in the universe, there are still many unanswered questions about supernovae. For the main types, core-collapse (type-II) and thermonuclear (type Ia), the driving mechanism and the evolutionary track towards the explosion are not yet satisfactorily comprehended. It is very clear, however, that weak interaction rates play a critical role in the evolution of both these types of supernovae and that the evolutionary tracks are sensitive to details of the weak reactions that take place in the evolving stars. Weak reaction rates on pf-shell nuclei (in type Ia supernovae, and in the pre-supernovae and collapse stages of Type II supernovae) and sdg-shell nuclei (in the collapse stage of type II supernovae) are particularly important [LAN01, BET79,HEG01,HIX03,JAN07,IWA99,BRA00]

After their cataclysmic demise, core-collapse supernovae can leave behind neutron stars and black holes. Neutron stars have recently drawn a lot of attention from nuclear astrophysics community: these objects of extremely high density are modeled to have a layered structure, and weak reactions in the crust of the neutron stars are considered to be of major importance for the heating [GUP06] and cooling processes through neutrino emission [SCH13].

The most important nuclear inputs for estimating weak reaction rates as a function of electron density and temperature are Gamow-Teller strength distributions. For most astrophysical applications, electron-captures (β^+ direction) are most important, but transition in the β^- direction should be known with reasonable precision as well. Direct information on Gamow-Teller strengths can be obtained from β-decay experiments, but only transitions associated with a positive Q-value window are accessible in such experiments, which is, in general, not sufficient. Extracting Gamow-Teller strengths from charge-exchange experiments at intermediate energies is the preferred method, relying on a well-tested proportionality between Gamow-Teller strength and charge-exchange

differential cross section at vanishing linear momentum transfer [TAD87,OST92,ZEG07,PER11].

For all of the above-mentioned phenomena where weak reactions play significant roles, it will be impossible to determine the relevant rates for even a significant fraction of nuclei based on experimental data. Not only do a very large number of nuclei play a role, in the hot environment of stellar interiors, weak reactions can take place on thermally excited states in the mother nuclei, which can only be studied in a very limited fashion in the laboratory. Consequently, the approach has been to perform targeted studies across relevant regions of the chart of the nuclei to benchmark theoretical approaches. Up to the pf-shell, configuration-interaction models with effective interactions are feasible [CAU99, HON04,HON05,POV01] and can be compared with calculations in Quasiparticle Random Phase Approximation (QRPA) [MOL90,NAB04,PAA09,DZH10,NIU11]. The QRPA calculations can be performed for nuclei beyond the pf-shell as well. For nuclei beyond the pf-shell, calculations in the framework of Shell-Monte Carlo combined with Random Phase Approximation [DEA98,JUO10] are also used.

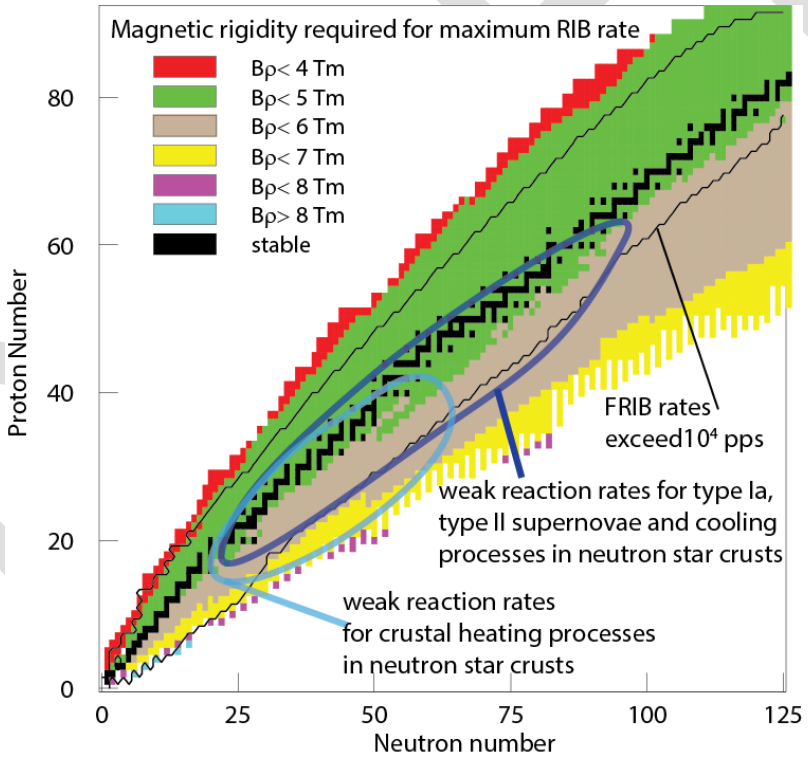

Fig. 5.4 Similar to Fig. 1.1: the rate contour (black) indicated the limit of 10^4 pps, the lower limit for which charge-exchange experiments with rare isotope beams in inverse kinematics are feasible. The blue contours roughly indicate the regions of interest for studying weak reaction rates in relevant astrophysical scenarios.

The focus of the experimental programs has so far been on stable pf-shell nuclei and a comprehensive overview and quantification of the uncertainties in EC rates based on

theoretical models by comparing to the data can be found in Ref. [COL12]. By combining the measurements on several nuclei across a region in the chart-of-nuclei with specific measurements key for understanding the nuclear structure near shell closures (in the case of the pf-shell, a measurement of the Gamow-Teller strength distribution from ^{56}Ni [SAS11,SAS12,LAN11]) definite statements about the quality of the theoretical models can be made [LIT14].

As discussed in section 2.7, the HRS at FRIB provides an ideal environment for charge-exchange experiments in inverse kinematics with rare-isotope beams. The beam energies of 170-200 MeV/u are an ideal match for studying charge-exchange reactions and expand the reach of the experiments as much as possible to the neutron-rich regions. Charge-exchange experiments require a beam intensity of at least 10^4 particles/s. In Fig. 5.4, the contour of that rate limit is superimposed on the chart of nuclei. Also shown are contours for the regions for which weak reaction rates are highly desirable. Clearly, nuclei are of interest for weak reaction processes in type Ia and type II supernovae, as well as nuclei of interest for cooling processes in neutron-star crusts and a large fraction of the nuclei of interest for heating of the crust.

Very recently [NOJ14], the advantage of combining charge-exchange experiments with high-resolution γ-ray spectroscopy has been demonstrated. This is particular important for experiments with astrophysical applications: detailed information about Gamow-Teller transitions to the lowest-lying states have strong impacts on the weak reaction rates, in particular when the stellar density is relatively low (e.g. during pre-supernovae evolution). The combination of the HRS with GRETA would be ideal for such experiments.

5.4. Astrophysical proton and α-decay branching ratios

Owing to their large universal abundances and small electric charge, a large number of astrophysically important reactions involve the radiative capture of either Hydrogen or Helium by heavier nuclei, many of which are very short-lived and cannot be made into targets. As it is very difficult to produce radioactive beams with sufficient intensity to measure these reaction cross sections directly, indirect methods must be brought to bear. If the radiative capture reactions of interest proceed dominantly via well separated, narrow resonances at astrophysical temperatures as is often the case in explosive scenarios, then the thermonuclear reaction rate can be calculated from the charged particle and radiative widths of the contributing resonances, or equivalently from their branching ratios and mean lifetimes. The HRS will enable the precise measurement of alpha- and proton-decay branching ratios via the population of excited states using two-body reactions in inverse kinematics.

In these measurements, the excitation energies in the compound nucleus are measured at the spectrometer's focal plane by the detection of the light ejectile of the two-body reaction. Simultaneously, the heavy residues created after proton- or α-decay are identified and counted with 100% geometric detection efficiency in a separate detector along with the radiative decay residues, yielding the decay branching ratio. Measurements of this kind have been performed for both α-decay [BAR03] and proton decay [BAR03a] using the Big Bite Spectrometer [BER95], a magnetic spectrometer with a large momentum acceptance of 10%, i.e. the same as that of the pre-conceptual design of the HRS shown in section 6.1. A large momentum acceptance is sometimes needed in these experiments because of the large magnetic rigidity difference between the decay residues and the light ejectile, which is often most copiously emitted at backward center-of-mass angles. Because the layout of the HRS involves two separate dipole stages (sweeper and spectrometer sections), there is also an opportunity to detect the heavy residues after the sweeper stage, allowing for an even large range of rigidity differences between the light ejectile and the heavy decay residues.
The intermediate energy beams which produce the desired forward focusing of the proton or α-decay residues also give rise to unwanted fragmentation reaction products. Both the beam and these fragmentation products must be stopped before they reach the focal plane detectors. Moreover, the α, proton, and radiative decay residues have vastly different specific ionizations, requiring a large dynamic range if they are all to be counted with the same detector. However, the position-sensitive focal plane detectors are only needed for the detection of the light ejectile and therefore provisions should be made to obscure any parts of the counters which would be subjected to large fragmentation product or beam fluxes. Many such problems can be avoided by employing an intermediate angular focus between the sweeper magnet and the main dipole magnet, at which slit systems could be deployed to block the passage of all but the light ejectiles and decay products of interest. The pre-conceptual layout of the HRS allows for the creation of such an intermediate focus.

6. The High Rigidity Spectrometer at FRIB

In this section, a summary of the pre-conceptual design study performed for the HRS is provided, as well as a possible location of the HRS at the FRIB facility. On the basis of these considerations, a first cost-estimate was made.

6.1. Pre-conceptual design

The High Rigidity Spectrometer (HRS) will enable the analysis of charged and uncharged reaction products stemming for an interaction of a rare-isotope beam with a stable

target. As such, it needs to separate neutrons, charged particles, and unreacted beam so that each can be detected with a specific detection system. In addition, ample space around the reaction target position needs to be available for the placement of auxiliary detection systems, such as GRETA for γ-detection. Based on the constraints and requirements set by the large variety of experiments that will be performed by the HRS, a pre-conceptual design study (first-order ion-optical calculation) was performed and a "base design" chosen, which served as basis for making initial cost estimates for the HRS. The pre-conceptual base design of the HRS is shown in Fig. 6.1. It has two main stages: a large-gap "sweeper" dipole magnet that will deflect all charged particles exiting the reaction target away from the beam axis. This enables the detection of neutrons in the forward direction (using the MoNA-LISA neutron detector array), including zero degree. The sweeper dipole is followed by the spectrometer section of the HRS that consists of quadrupole focusing elements followed by a dipole stage, comprised of two dipole magnets.

The basic requirements of the HRS have been established by the HRS working group of the FRIB user organization over the course of several years, during users meetings and dedicated workshops, the latest of which was held in July 2014. The HRS pre-conceptual design strives to accommodate these requirements.

The basic requirements are:

- Maximum rigidity at least 7 Tm
- Momentum resolution of at least 1:1000
- Large acceptance (>5 msr, but preferably >10 msr angular, 10% momentum)
- 16° opening angle for neutrons (chosen based on the benchmark that 100% acceptance for neutrons emitted for 2 MeV decay energies from a 150 MeV/nucleon ^{40}Al particles is achieved)
- Neutron flight path of up to 15 m
- Space around the reaction target to accommodate auxiliary detector systems
- The capability to uniquely identify isotopes up to mass ~200.

The base concept

The sweeper dipole for the base concept is a superconducting large-gap dipole that provides a 30° bend for up to 8 Tm rigidity. The required maximum field strength is 2.1 T. To calculate standard acceptances, the reaction target is placed 1 m upstream of the sweeper's field edge. At that distance, a 0.60 m sweeper dipole gap offers an 11.8° vertical opening for neutrons. This fully illuminates a 1.6 m tall neutron detector at 8 m distance from the reaction target. Of course, the target can be moved closer to the sweeper dipole (as is routinely done for experiments at the existing NSCL Sweeper dipole magnet): a 16° vertical opening requires placing the reaction target 0.22 m in front of the sweeper dipole magnet.

The neutron flight path from the target to the fast neutron detectors can be adjusted to achieve a good balance between neutron detection acceptance and the required timing resolution.

The acceptance for charged particles is determined by the bore diameter of the focusing quadrupoles placed after the sweeper magnet. For the base concept, we chose to use quadrupoles that are being designed for the ARIS preseparator for FRIB (FSQ7, FSQ8), which are suitable in their specifications. These quadrupoles are specified to have a full aperture of 0.4 m. This includes multipoles and a larger aperture of up to 0.5 m can be achieved if the multipoles are left out, which could be done for some of the quadrupoles. An alternative to these quadrupoles would be to use a warm-iron design (such as FSQ4 of the FRIB separator), which offers an aperture of 0.58 cm. Such consideration must be studied in more detail on the basis of ion-optical design studies that include higher-order ion-optical calculations.

The magnets shown in Fig. 6.1 are not based on full magnet designs, but roughly indicate the physical dimensions. Some of the dimensions of the beam line elements will have an impact on the performance of the HRS, e.g. the outer dimension of the quadrupole magnets can limit the angular acceptance for neutrons. Fig. 6.1 also shows the location of the neutron detector array MoNA-LISA (at 15 m from the target) and indicates a neutron cone with a 16° opening angle.

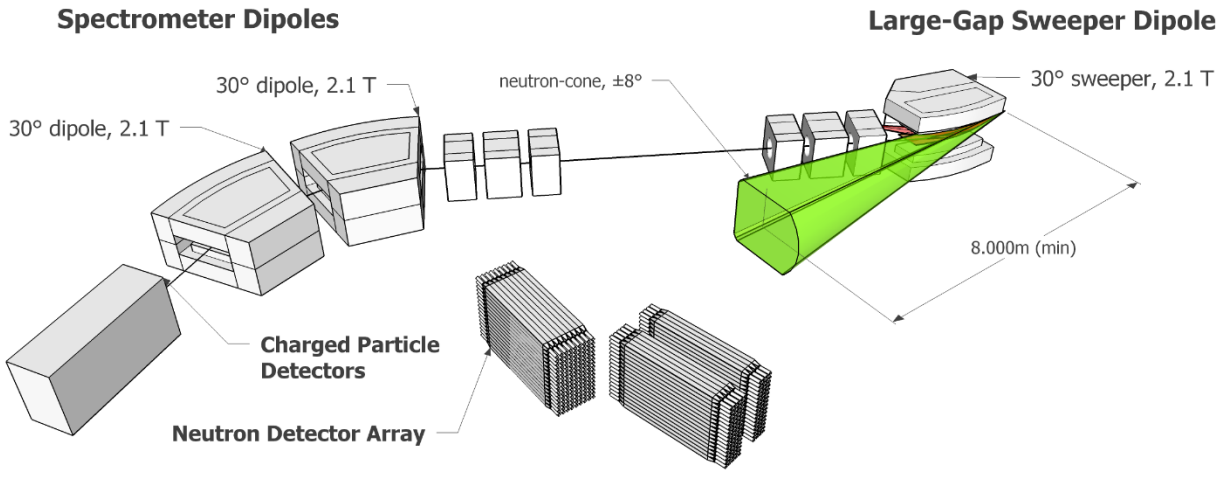

Fig. 6.1 Schematic view of the base concept of the High Rigidity Spectrometer.

An envelope plot of the first-order ion optical calculation for the HRS base concept is shown in Fig. 6.2. The presented ion optics assumes a 1 mm diameter source at the object (reaction target) of the HRS emitting into a cone of 80 mrad opening, placed 1 m in front

of the sweeper dipole edge. Of course, the emittance of rare-isotope beams transported from the FRIB fragment separator to the HRS will affect the resolutions that can be achieved. Therefore, detectors to track the incoming beam will be used to counter the effects if the sizeable beam emittance. The charged-particle beam (consisting of charged reaction products) is deflected by the sweeper dipole and directed into the first focusing triplet. The sweeper dipole is a large-gap superconducting 30° dipole. Ideally, the sweeper should be a C-type magnet with one side open so that neutrons can be detected at larger angles. It will also be designed to accommodate the detection of light charged particles with up to half the rigidity of the charged reaction products.

Behind the sweeper magnet, the beam is focused in a dispersive plane downstream of the triplet. At this position, there is a small dispersion (less than 1 cm/%). This focal plane can be used for particle tracking and for blocking of unreacted beam. The latter is very important for experiments in which the reaction products of interest have rigidities that are relatively close to that of the unreacted beam, and the beam intensity is too high to transmit to the focal-plane detectors after the spectrometer section of the HRS. Shortly after the intermediate focus, a second quadrupole triplet focuses the beam into the spectrometer dipole magnets. The two dipole magnets are identical and bend the beam by 30° each. They have a vertical gap of 0.12 m. Downstream of the spectrometer dipoles is the final focus, which will be the location of the charged particle detectors for tracking and particle identification. This focal plane has a large dispersion (more than 5 cm/%), which is needed to achieve the required resolution. The flight path from the object to the final focus is about 24 m.

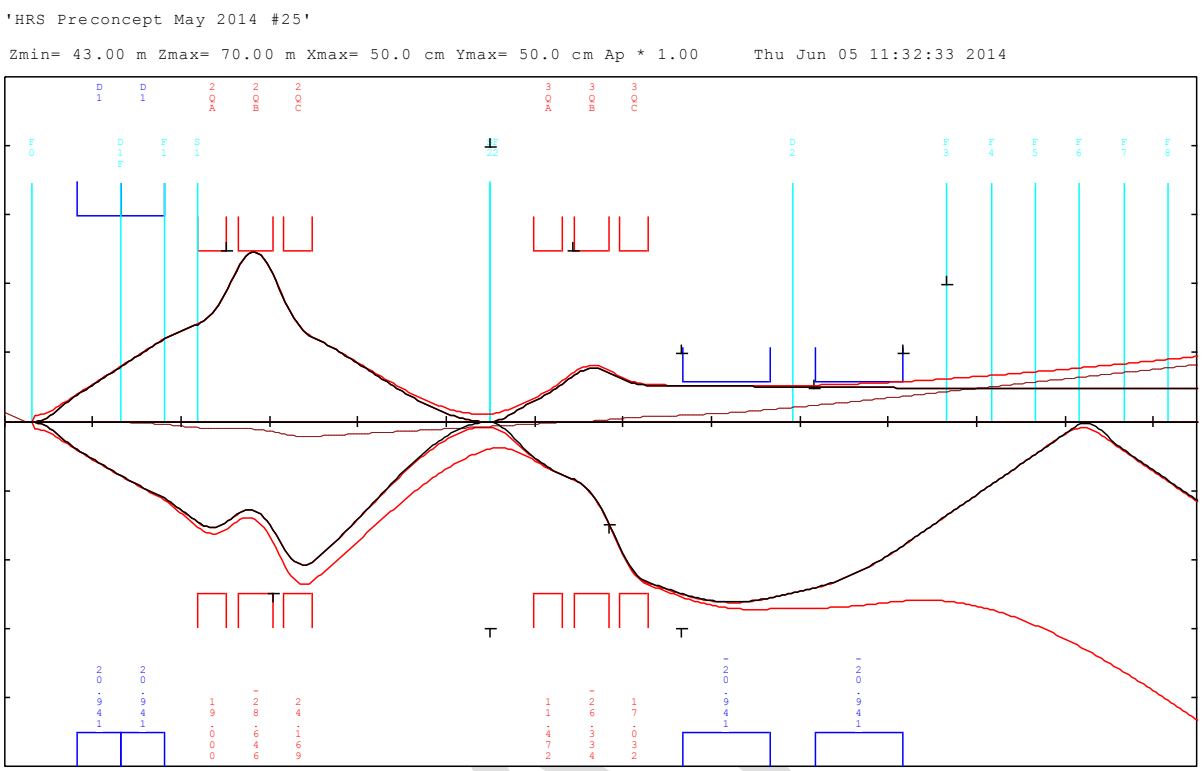

Fig. 6.2 First-order ion optical calculation of the HRS reaction target to final focal plane section. The black line indicates the envelope of an 80 mrad by 80 mrad beam with no momentum dispersion. The two red lines represent envelopes of a beam with ten times the beam spot size or 10% total momentum spread.

In summary, the pre-conceptual design of the HRS spectrometer has the following properties:

- It consists of one dipole sweeper magnet, two quadrupole triplets, and two dipole spectrometer magnets
- It has a maximum magnetic rigidity: 8 Tm
- Acceptance: 80 mrad by 80 mrad (charged particles), 10% dp/p, ±6° (vertical, neutrons)
- Image after sweeper; Resolution: 5000; dispersion at focal plane: 7 cm/%.
- Sweeper: 30° bending angle, 2.1 T max. field, 0.6 m gap. Ideally C-type magnet.
- Main dipoles: 2×30° bending angle, 2.1 T max. field, 0.12 m gap.
- Quadrupoles: based on FSQ7/8 design for FRIB separator, ~0.50 m max. bore (without multipoles).

The angular acceptance of the base design (~6 msr) is somewhat lower than preferable. To mitigate this situation, focusing quadrupole magnets would have to be placed between the target and the sweeper dipole stage, as is the case for the existing S800 spectrograph at NSCL. This would not be feasible for experiments that require a large

acceptance for fast neutrons in MoNA-LISA. Nevertheless, the placement of such focusing quadrupole magnets prior to the sweeper dipole could become an option for experiments that require a large angular acceptance for the HRS.

Design alternative for the sweeper dipole magnet

One particularly interesting design alternative considered during the pre-conceptual stage, was to replace the sweeper dipole magnet with high-field (6-8 T field) magnet. The length of the magnet could be reduced if a high field is applied to bend the charged particles, with the limitation that the quadrupole magnets after the sweeper dipole cannot interfere with the fast neutrons directed at the neutron-detector array. This limitation requires that the bending of the sweeper dipole is increased (to 45° for a 6 T sweeper dipole magnet, for a field length of 1 m). By reducing the length of the sweeper dipole, the quadrupole magnets after the sweeper can be placed closer to the target, hence improving the acceptance of the full HRS. This feasibility of this design alternative and the impact of larger fringe fields produced by a high-field dipole magnet will require further investigation in future design stages.

6.2. Possible location of the HRS at FRIB

As part of the pre-conceptual design of the HRS at FRIB, the location of the experimental vault for the device was considered. The considerations tentatively focused on placing the HRS in a new high-bay area, situated just south of the current S2/S3 fast-beam areas at NSCL, as shown in Fig. 6.3. In the choice for this location, the ability to place the auxiliary detection systems was an important boundary condition, and GRETA and MoNA-LISA were chosen as primary examples due to their significant footprint.

A first order ion-optical design for the beam line transporting rare isotopes from the FRIB fragment separator to the HRS was performed, based on projected beam emittances of rare-isotope beams produced in the fragment separator (Horizontal beam envelope: ±1 mm, ±36 mrad; vertical beam envelope: ±5 mm, ±20 mrad, dp/p=±2%). It is important to ensure that the acceptance of the beam line magnets used in the transport line is sufficient to ensure a high transmission to the HRS. In the conceptual layout, quadrupoles (6) of the same type as used in the fragment separator were assumed. Also considered were the need to replace the switching dipole magnet at the end of the fragment separator, and an additional dipole bending magnet and a quadrupole triplet placed prior to the HRS target station. The use of the dipole just prior to the target provides the opportunity to tune the rare-isotope beams from the fragment separator to the HRS in dispersion-matched mode, which can be useful in experiments where very high momentum resolutions must be achieved without beam tracking, or for experiments that require a well-localized image of the beam after the sweeper stage of the spectrometer,

so that the unreacted beam can be blocked even if the reaction products of interest are closely situated to the unreacted beam.

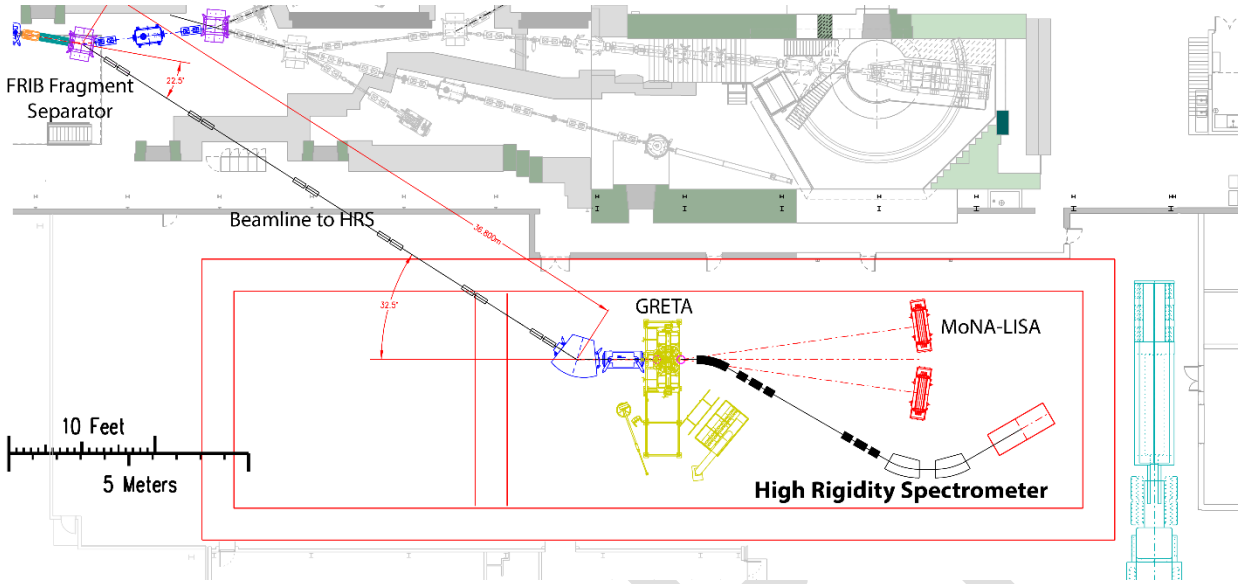

Fig. 6.3 Possible Layout for the experimental area for the High Rigidity Spectrometer at FRIB in a new high-bay, located south of the present NSCL fast beam areas (S2/S3 vaults). The large-acceptance beam line, connecting the FRIB fragment separator to the HRS was included in the cost estimate.

6.3. Cost estimates & time line for the HRS and associated infrastructure.

The cost estimates for the HRS, as well as the beam line from the fragment separator to the HRS, associated technical infrastructure, and detector systems were estimated based on the pre-conceptual design consideration discussed above. These estimates include costs associated with labor for design, manufacturing, installation and project management. Also included were 30% contingencies for magnets (and associated infrastructure) with a technical scope that is well established. Contingencies were set to 50% for the sweeper dipole magnet and the 2 spectrometer dipole magnets, for which the uncertainties in the technical scope were considered to be larger. In the numbers presented in table 1, costs for the construction of a new high bay are not included. These were estimated at $10M ($1M contingency), including the necessary utility infrastructure, radiation shielding and interlocks, and a 40T overhead crane.

TABLE 2 SUMMARY OF THE COST ESTIMATES FOR THE CONSTRUCTION OF THE HIGH RIGIDITY SPECTROMETER AT FRIB

	Equipment	*Labor*	*Total*	*Including contingency*	*Note*
Beam line	$3.9M	$4.8M	$8.7M	$11.4M	Includes switching dipole, 6 beamline doublets, one beam line dipole and quadrupole triplet, and associated infrastructure
HRS	$4.1M	$8.3M	$12.4M	$17.8M	Includes sweeper dipole, 2 quadrupole triplets and 2 spectrometer dipoles, and associated infrastructure and detectors
Total	**$8.0M**	**$13.1M**	**$21.1M**	**$29.1M**	

The design of the High Rigidity Spectrometer is envisioned to start in 2017 with the goal to initiate experiments with the device during early operations of FRIB. A very significant fraction of the experiments that can be performed with the HRS are based on proven principles and a vibrant program at the early stages of operations at FRIB can very quickly lead to high-impact scientific results.

References

[ABR12] S. Abrahamyan et al., Phys. Rev. Lett. 108, 112502 (2012)
[ADR05] P. Adrich et al., Phys. Rev. Lett. 95, 132501 (2005)
[ALA96] N. Alamanos and P. Chomaz-Roussel, Ann. Phys. Fr. 21, 601 (1996)
[ALK96] J. S. Al-Khalili and J. A. Tostevin, Phys. Rev. Lett. 76, 3903 (1996)
[ALK97] G. D. Alkhazov et al., Phys. Rev. Lett. 78, 2313 (1997)
[AMO06] K. Amos, W.A. Richter, S. Karataglidis and B.A. Brown, Phys. Rev. Lett. 96, 032503 (2006).
[AND10] A. Andreyev et al., Phys. Rev. Lett. 105, 252502 (2010)
[AST14] Whitepaper on Nuclear Astrophysics, to be published
[AUM13] T. Aumann, C. A. Bertulani, and J. Ryckebusch, Phys. Rev. C 88, 064610 (2013)
[BAU05] T. Baumann et al., Nucl. Instr. and Meth. A543, 517 (2005)
[BAU12] T. Baumann, A. Spyrou and M. Thoennessen, Rep. Prog. Phys. 75, 036301 (2012)
[BAZ09] D. Bazin et al., Phys. Rev. Lett. 102, 232501 (2009)
[BEC13]B. Becker, et al., Phys. Rev. C 87, 014617 (2013)
[BEN07] M.A. Bentley and S.M. Lenzi, Prog. in Particle and Nucl. Phys. 59, 497 (2007)
[BER83] A.M. Bernstein et al., Comments Nucl. Part. Phys. 11, 203 (1983)
[BER84] J. F. Berger, M. Girod, D. Gogny, Nucl. Phys. A, 428 (1984) 23
[BER88] Carlos A. Bertulani and Gerhard Baur, Phys. Rep. 163, 299 (1988)
[BER95] A. M. van den Berg, Nucl. Instrum. Methods Phys. Res. B 99, 637 (1995)
[BET79] H. A. Bethe, G. E. Brown, J. Applegate, and J. M. Lattimer, Nucl. Phys. A 324, 487 (1979)
[BLA07] B. Blank and M. Borge, Prog. in Part. and Nucl. Phys. 60(2) 403 (2007)
[BRA00] F. Brachwitz et al., Astrophys. J. 536, 934 (2000)
[BRO00] B.A. Brown, Phys. Rev. Lett. 85, 5296 (2000)
[BRO01] B.A. Brown. Prog. Part. Nucl. Phys. 47, 517 (2001).
[BRO09] J.R. Brown et al, Phys. Rev. C 80, 011306(R) (2009)
[BRO13] B.A. Brown, Phys. Rev. Lett. 111, 232502 (2013)
[CAA13] M. Caamano et al, Pys. Rev. C 88, 024605 (2013)
[CAM06] C. M. Campbell et al., Phys. Rev. Lett. 97, 112501 (2006)
[CAR10] A. Carbone et al., Phys. Rev. C 81, 041301 (2010)
[CAU99] E. Caurier et al., Nucl. Phys. A 654, 973c (1999)
[CED11] B. Cederwall et al., Nature Vol 469, 68 (2011)
[CHE03] Lie-Wen Chen, V. Greco, C. M. Ko, and Bao-An Li, Phys. Rev. C 68, 014605 (2003)
[CHR12] G. Christian et al., Phys. Rev. Lett. 108, 032501 (2012)
[CLA03] B.C. Clark, L.J. Kerr and S. Hama, Phys. Rev. C 67, 054605 (2003)
[COL12] A. L. Cole et al., Phys. Rev. C 86, 015809 (2012)
[COL14] G. Colò, U. Garg, and H. Sagawa, Eur. Phys. J A 50, 26 (2014)
[COU12] D. Coupland, PhD thesis, MSU, (2012)
[COW98] A. A. Cowley et al., Phys. Rev. C 57, 3185 (1998)
[CRA14] H. L. Crawford et al., Phys. Rev. C 89, 041303(R) (2014)
[DAN02] P. Danielewicz, R. Lacey, W.G. Lynch, Science 298, 1592 (2002)
[DAN03] P. Danielewicz, Nucl. Phys. A 727, 233 (2003)
[DAN13] P. Danielewicz, J. Lee, Nucl. Phys. A (2014)
[DAV03] B. Davids et al., Phys. Rev. C 67, 065808 (2003)

[DAV03a] B. Davids et al., Phys. Rev. C 68, 055805 (2003)
[DEA98] D.J. Dean et al., Phys. Rev. C 58, 536 (1998)
[Den08] D. H. Denby et al., Phys. Rev. C 78, 044303 (2008)
[DIC01] W.H. Dickhoff, C. Barbieri, Prog. Part. Nucl. Phys. 52, 377 (2004)
[DIT10] M, Di Toro, V, Baran, M, Colonna, et al. J. Phys. G,37, 083101 (2010)
[DOO13] P. Doornenbal et al., Phys. Rev. Lett. 111, 212502 (2013)
[DZH10] A. A. Dzhioev et al., Phys. Rev. C 81, 015804 (2010)
[EJI05] H. Ejiri, J. Phys. Soc. Jpn 74, 2101 (2005)
[EKM04] J. Ekman et al., Phys. Rev. Lett. 92 132502 (2004).
[ELL02] S.R. Elliot and P. Vogel, Annu. Rev. Nucl. Part. Sci. 52, 115 (2002)
[ERE86] A. Erell et al., Phys. Rev. C 34, 1822 (1986)
[ERL12] Erler et al., Nature 486, 509 (2012) and references therein.
[ERL12] J. Erler et al, Phys. Rev. C 85, 025802 (2012)
[EST11] A.Estrade et al., Phys. Rev. Lett. 107, 172503 (2011)
[FAM06] M.A. Famiano et al., Phys. Rev. Lett. 97, 052701 (2006)
[FLA12] F. Flavigny et al., Phys. Rev. Lett. 108, 252501 (2012)
[FRA05] S. Fracasso and G. Colò, Phys. Rev. C 72, 064310 (2005)
[FRA85] M.A. Franey and W.G. Love, Phys. Rev. C 31, 488 (1985)
[FRO93] S. V. Förtsch et al., Phys. Rev. C 48, 743, 1993
[FUC06] C. Fuchs, Prog. Part. Nucl. Phys. 56, 1 (2006)
[FUJ11] Y. Fujita and B. Rubio and W. Gelletly, Prog. Part. Nucl. Phys. 66, 549 (2011)
[GAD05] A. Gade et al., Phys.Rev. C 71, 051301(R) (2005)
[GAD06] A. Gade et al., Phys. Rev. C 74, 021302(R) (2006)
[GAD07] A. Gade et al., Phys. Rev. C 76 024317 (2007)
[GAD08a] Alexandra Gade and Thomas Glasmacher, Prog. in Part. and Nucl. Phys. 60, 161 (2008)
[GAD08b] A. Gade et al., Phys. Rev. C 77, 044306 (2008)
[GAN12] S. Gandolfi, J. Carlson, S. Reddy, Phys. Rev. C 85,032801(R) (2012)
[GAU12] L.Gaudefroy et al., PRL 109 202503 (2012)
[GLA98] T. Glasmacher, Annu. Rev. Nucl. Part. Sci. 48, 1 (1998)
[GOR13] S. Goriely et al, Phys. Rev. Lett. 111, 242502 (2013)
[GOU05] H. Goutte, et al., Phys. Rev. C 71, 024316 (2005)
[GRA06] H. Grawe et al., Eur. Phys. Jour. A 27, 257 (2006)
[GRI11] G. F. Grinyer et al., Phys. Rev. Lett. 106, 162502 (2011)
[GRI12] G. F. Grinyer et al., Phys. Rev. C 86, 024315 (2012)
[GRZ98] R. Grzywacz, et al., Phys. Rev. Lett. 81, 766 (1998)
[GUE09] C. J. Guess et al., Phys. Rev. C 80, 024305 (2009)
[GUI13] S. Guillot, M. Servillat, N.A. Webb, R.E. Rutledge, Astrophys. J. 772, 7 (2013)
[GUP06] Sanjib Gupta et al., Astrophys. J. 662, 1188 (2006)
[HAN01] P. G. Hansen and B. M. Sherrill. Nucl. Phys. A693, 133 (2001).
[HAN03] P.G. Hansen, J.A. Tostevin, Annu. Rev. Nucl. Part. Sci. 53, 221 (2003)
[HAR01] M.N. Harakeh and A. van der Woude, Giant Resonances, Fundamental High-Frequency Modes of Nuclear Excitations, Oxford Studies in Nuclear Physics 24, Clarendon Press, Oxford, 2001
[HAM13] H.-W. Hammer, A. Nogga, and A. Schwenk, Rev. Mod. Phys. 85, 197 (2013).

[HAT97] K. Hatanaka, et al., Phys. Rev. Lett. 78, 1014 (1997)
[HEB10] K. Hebeler, A. Schwenk, Phys. Rev. C 82, 014314 (2010)
[HEG01] A. Heger, S.E. Woosley, G. Martinez-Pinedo, K. Langanke, Ap. J. 560, 307 (2001)
[HIN12] N.Hinohara et al., Prog.Theo.Phys.196 (2012) 328
[HIX03] W.R. Hix et al., Phys. Rev. Lett. 91, 201102 (2003)
[HOF08] C. R. Hoffman et al., Phys. Rev. Lett., 100, 152502 (2008)
[HOF09] C. R. Hoffman et al., Phys. Lett. B 672, 17 (2009)
[HOF11] C. R. Hoffman et al., Phys. Rev. C 83, 031303(R) (2011)
[HOL12] J. D. Holt et al., J. Phys. G: Nucl. Part. Phys. 39, 085111 (2012)
[HOL14] J. D. Holt et al., arXiv.1405.7602 (2014)
[HON04] M. Honma, T. Otsuka, B. A. Brown, and T. Mizusaki, Phys. Rev. C 69, 034335 (2004)
[HON05] M Honma, T Otsuka, T. Mizusaki, M. Hjorth-Jensen and B. A. Brown, J. Phys. G 20, 7 (2005)
[HON13] J. Hong and P. Danielewicz, ArXiv e-prints (2013)
[HOR01] C.J. Horowitz et al., Phys. Rev. Lett. 86, 5647 (2001)
[HOR14] C.J. Horowitz et al., J. Phys. G (2014)
[HUC85] A. Huck et al., Phys. Rev. C 31, 2226 (1985)
[IRO86] F. Irom et al., Phys. Rev. C 34, 2231 (1986)
[IWA99] K. Iwamoto et al., Astrophys. J. Suppl. 125, 439 (1999)
[JAN07] H.-T. Janka, K. Langanke, A. Marek, G. Martínez-Pinedo, and B. Müller, Phys. Rep. 442, 38 (2007)
[JAN13] M. Jandel, et al., Los Alamos Report LA-UR-12-24975, 2013
[JEN11] Ø. Jensen, G. Hagen, M. Hjorth-Jensen, B. Alex Brown, and A. Gade, Phys. Rev. Lett. 107, 032501 (2011).
[JIA07] Wei-Zhou Jiang, Bao-An Li, and Lie-Wen Chen, Phys. Rev. C 76, 044604 (2007)
[JUO10] A. Juodagalvis et al., Nucl. Phys. A848, 454 (2010)
[KAR02] K. Amos, B.A. Brown and P.K. Deb, Phys. Rev. C65, 044306 (2002)
[KOB12] N. Kobayashi et al., Phys. Rec. C. 86, 054604 (2012)
[KOH13] Z. Kohley et al., Phys. Rev. C 87, 011304(R) (2013)
[KOH13] Z. Kohley et al., Phys. Rev. C 88, 041601 (2013)
[KOH13a] Z. Kohley et al., Phys. Rev. Lett. 110, 152501 (2013)
[KON03] A. J. Koning and J. P. Delaroche, Nucl. Phys. A713, 231 (2003)
[KOR12] O. Korobkin et al, Mon. Not. R. Astron. Soc. 426, 1940 (2012)
[KRA88] G.J. Kramer et al., Nucl. Phys. A 477, 55 (1988)
[KRA99] A. Krasznahorkay et al., Phys. Rev. Lett. 82, 3216 (1999)
[KRE95] G. Krein et al., Phys. Rev. C 51, 2646 (1995)
[LAN01] K. Langanke and G. Martinez-Pinedo, Nucl. Phys. A673, 481, (2000) and
At. Nucl. Data Tables 79, 1 (2001)
[LAN03] K. Langanke, G. Martinez-Pinedo, Rev. Mod. Phys. 75, 819 (2003)
[LAN11] Physics Viewpoint: Recreating a Stellar Electron Catch, Karlheinz Langanke, Physics 4, 91 (2011)
[LAP14] Large-Area Picosecond Photo-Detectors Project http://psec.uchicago.edu/
[LAT01] J.M. Lattimer, M. Prakash, ApJ, 550, 426 (2001)
[LAT04] J.M. Lattimer, M. Prakash, Science 304, 536 (2004)
[LAT13] J. M. Lattimer and Y. Lim, ApJ 771, 51 (2013)
[LI05] Bao-An Li and Lie-Wen Chen, Phys. Rev. C 72, 064611 (2005)
[LI05] B.A. Li, L.W. Chen, Phys. Rev. C 72, 064611 (2005)

[LI05b] B.A. Li, G.C. Yong, W. Zuo, Phys. Rev. C71, 014608 (2005)
[Li07] T. Li et al., Phys. Rev. Lett. 99, 162503 (2007)
[Li08] Bao-An Li et al., Phys. Rep. 464, 113 (2008)
[Li93] G. Q. Li and R. Machleidt, Phys. Rev. C 48, 1702 (1993)
[Li94] G. Q. Li and R. Machleidt, Phys. Rev. C 49, 566 (1994)
[LIT14] E Litvinova, BA Brown, DL Fang, T Marketin, RGT Zegers, Phys. Lett. B 730, 307 (2014)
[LOC14] Bui Minh Loc, Dao T. Khoa, and R. G. T. Zegers, Phys. Rev. C 89, 024317 (2014)
[LOV81] W. G. Love and M. A. Franey, Phys. Rev. C 24, 1073 (1981)
[LRP07] The Frontiers of Nuclear Science, A long Range Plan, The Nuclear Science Advisory Committee, (2006)
[LUN12] E. Lunderberg et al., Phys. Rev. Lett., 108, 142503 (2012)
[LUT03] B. Luther et al., Nucl. Instr. and Meth. A505, 33 (2003)
[MAD82] D. G. Madland, J. R. Nix, Nuclear Science and Engineering 81, 213 (1982)
[MAM13] J. Mammei et al., CREX: PARITY-VIOLATING MEASUREMENT of the WEAK CHARGE DISTRIBUTION of 48Ca to 0.02 fm ACCURACY
[MAR99] F. Marechal et al., Phys. Rev. C60, 034615 (1999)
[MEH12] R. Meharchand et al., Phys. Rev. Lett. 108, 122501 (2012)
[MEI13] Z. Meisel and S. George, IJMS 349, 145 (2013)
[Moe95] P. Moeller, J.R. Nix, and W.J. Swiatecki, At. Data Nucl. Data Tables 59 (1995) 185
[MOE09] P. Moeller et al, Phys. Rev. C 79, 064304 (2009)
[MOL01] P. Moller, et al., Nature 409, 785 (2001)
[MOL90] P. Möller and J. Randrup, Nucl. Phys. A514, 1 (1990)
[MON08] C. Monrozeau et al., Phys. Rev. Lett. 100, 042501 (2008)
[MRI09] MRI-Consortium: Development of a Neutron Detector Array by Undergraduate Research Students for Studies of Exotic Nuclei, NSF grants 0922335, 0922409, 0922446, 0922462, 0922473, 0922537, 0922559, 0922622, and 0922794
[NAB04] J.-U. Nabi and H. V. Klapdor-Kleingrothaus, At. Data Nucl. Data Tables 88, 237 (2004)
[NAK99] S. Nakayama et al., Phys. Rev. Lett. 83, 690 (1999)
[NAR07] B.S. Nara Singh et al., Phys. Rev. C 75, 061301(R) (2007)
[NIU11] Y. F. Niu, N. Paar, D. Vretenar, and J. Meng, Phys. Rev. C 83, 045807 (2011)
[NOJ14] S. Noji et al., Phys. Rev. Lett 112, 252501 (2014)
[NRC13] National Research Council. *Nuclear Physics: Exploring the Heart of Matter*. Washington, DC: The National Academies Press, 2013
[OBE11] A. Obertelli et al, Phys. Lett. B 701, 417–421 (2011)
[OBS13] A. Obserstedt, et al., Phys. Rev. C 87, 051602(R) (2013)
[OST92] F. Osterfeld, Rev. Mod. Phys. 64, 491 (1992)
[OTS10] T. Otsuka et al., Phys. Rev. Lett. 105, 032501 (2010)
[OZA01] A. Ozawa, T. Suzuki and I. Tanihata, Nucl. Phys. A 693, 32 (2001)
[PAA09] N. Paar, G. Colò, E. Khan, and D. Vretenar, Phys. Rev. C 80, 055801 (2009)
[PAN05] I. V. Panov et al, Nucl. Phys. A 747, 633 (2005)
[PAS11] K. Paschke, K. Kumar R. Michaels, P.A.Souder, G.M. Urciuoli et al., JLAB Exp E12-11-101, PREX-II: PRECISION PARITY-VIOLATING MEASUREMENT OF THE NEUTRON SKIN OF LEAD
[PAT12] D. Patel et al., Phys. Lett. B 758, (2012)
[PEL13] E. Pellereau et al, EPJ Web of Conf. 62, 06005 (2013)
[PER11] G. Perdikakis et al., Phys. Rev. C 83, 054614 (2011)

[PFU12] M. Pfutzner et al. Rev. Mod. Phys. 84, 567 (2012).
[POV01] A. Poves, J. Sánchez-Solano, E. Caurier, and F. Nowacki, Nucl. Phys. A694, 157 (2001)
[RIL05] L. A. Riley et al., Phys. Rev. C72, 024311 (2005)
[RIB07] Report to NSAC of the Rare-Isotope Beam Task Force
[ROG11] A.M. Rogers et al., Phys. Rev. Lett. 106, 252503 (2011)
[ROH04] D. Rohe et al., Phys. Rev. Lett. 93, 182501 (2004)
[SAG07] H. Sagawa, S. Yoshida, X.-R. Zhou, K. Yako and H. Sakai, Phys. Rev. C 76, 024301 (2007)
[SAM06] F. Sammarruca and P. Krastev, Phys. Rev. C 73, 014001 (2006)
[SAS11] M. Sasano et al., Phys. Rev. Lett. 107, 202501 (2011)
[SAS12] M. Sasano et al., Phys. Rev. C 86, 034324 (2012)
[SAS12a] Yoshiko Sasamoto, Study of the isovector non-spin-flip monopole resonance via the super allowed Fer
Dissertation, University of Tokyo, and to be published.
[SAV13] D. Savran, T. Aumann, and A. Zilges, Prog. Part. Nucl. Phys. 70, 210 (2013)
[SCH00] H. Scheit et al., Phys. Rev. C63, 014604 (2000)
[SCH01] K.-H. Schmidt, Nucl. Phys. A 693, 169 (2001)
[SCH02] H. Schatz et al, Astrophys. Jour. 579, 626 (2002)
[SCH07] A. Schiller et al., Phys. Rev. Lett. 99, 112501 (2007)
[SCH13] H. Schatz et al., Nature (London) 505, 62 (2013)
[SCH98] C. Scheidenberger et al., Nucl. Instr. And Meth, in Phys. Res. B 142, 441 (1998)
[SCO14] M. Scott et al., NSCL-experiment E11021, Search for the Isovector Giant Monopole Resonance via the ^{28}Si(^{10}Be,^{10}B+g) reaction at 100 MeV/u, to be published
[SPY12] A. Spyrou et al., Phys. Rev. Lett. 108, 102501 (2012)
[STE05] A.W. Steiner, M. Prakash, J.M. Lattimer, P.J. Ellis, Phys. Rep. 411, 325 (2005)
[STE13] D. Steppenbeck et al., Nature 502, 207 (2013)
[STE13a] I. Stetcu, et al., Phys. Rev. C 88 (2013) 044603
[SUC14] S.Suchyta et al., Phys. Rev. C89 (2014) 021301(R)
[SUL11] V. Suleimanov, J. Poutanen, M. Revnivtsev, K. Werner, Astrophys. J. 742, 122 (2011)
[SUZ13] H. Suzuki et al., Phys. Rev. C88, 024326 (2013)
[SUZ90] Yasuyuki Suzuki, Kiyomi Ikeda and Hiroshi Sato, Prog. Theor. Phys. 83, 180 (1990).
[SUZ95] T. Suzuki et al., Phys. Rev. Lett. 75, 3241 (1995)
[TAD87] T. D. Taddeucci et al., Nucl. Phys. A469, 125 (1987)
[TAK09] S. Takeuchi et al., Phys. Rev. C79, 054319 (2009)
[TAL11] P. Talou, et al., Phys. Rev. C 83, 064612 (2011)
[TAL12] P. Talou, et al., Proceedings of the 5th International Conference on Fission, Sanibel Island, Nov. 2012 (pp. 581-588)
[TAM11] A. Tamii et al., Phys. Rev. Lett. 107, 062502 (2011)
[TAN92] I. Tanihata, D. Hirata, T. Kobayashi, S. Shimoura, K. Sugimoto and H. Toki, Phys. Lett. B 289, 261 (1992)
[THI83] F.-K. Thieleman et al, Z. Phys. A 309, 301 (1983)
[THO04] M. Thoennessen, Rep. Prog. Phys. 67, 1187 (2004)
[TOS01] J.A. Tostevin, Nuclear Phys. A 682, 320c (2001)
[TOS99] J.A. Tostevin, J. Phys. G 25, 735 (1999)
[TSA09] M.B. Tsang et al., Phys. Rev. Lett. 102, 122701 (2009)
[TSA12] M.B. Tsang et al., Phys. Rev. C 86, 015803 (2012)
[TSU14] Y. Tsunoda et al., Phys. Rev. C89, 031301(R) (2014)

[ULL14] J. L. Ullmann, et al., Phys. Rev. C 89, 034603 (2014)
[VAN14] M. Vandebrouck et al., PRL 113, 032504 (2014)
[VIL04] A.R. Villarreal, T.E. Strohmayer, ApJ, 614, L121 (2004)
[VOG12] R. Vogt, et al., Phys. Rev. C 85 (2012) 024608
[VRE03] D. Vretenar, N. Paar, T. Niksic, P. Ring, Phys. Rev. Lett. 91, 262502 (2003)
[WAR06] D.D. Warner, M.A. Bentley, and P. Van Isacker, Nature Physics 2, 311 (2006)
[WAT13] H. Watanabe et al., Phys. Rev. Lett. 111, 152501 (2013)
[WIM14] K. Wimmer et al., to be submitted to Nucl. Intr. and Meth.
[XIA08] Zhigang Xiao et al., Phys. Rev. Let. 102, 062502 (2009)
[YAK06] K. Yako, H. Sagawa, and H. Sakai, Phys. Rev. C 74, 051303(R) (2006)
[YOS04] Satoshi Yoshida and Hiroyuki Sagawa, Phys. Rev. C 69, 024318 (2004)
[YOU97] D.H. Youngblood, H.L. Clark, Y.W. Lui, Phys. Rev. Lett. 82, 691 (1999)
[YUR04] K. L. Yurkewicz et al., Phys. Rev. C 70, 054319 (2004)
[ZEG07] R.G.T Zegers et al., Phys. Rev. Lett. (2007)
[ZEG10] R.G.T. Zegers et al., Phys. Rev. Lett. 104, 212504 (2010)
[ZEL06] Vladimir Zelevinsky and Alexander Volya, AIP Conf. Proc. 819, 493 (2006)
[ZHA13] Z. Zhang, L.W. Chen, ArXiv e-prints (2013)
[ZHA14] Y.X. Zhang, M.B. Tsang, Z.X Li, and H. Liu, Phys. Lett. B 732, 186 (2014)

Contributors & Workshop participants

The following people serve as conveners for the HRS working group, participated in the July 2014 workshop "A High Rigidity Workshop for FRIB" and/or contributed to this document.

Matt Amthor
Thomas Aumann
Thomas Baumann
Daniel Bazin
Saul Beceiro Novo
Georg Berg
Georg Bollen
Rose Blanchard
Mustapha Brahim
James Brown
Earl Burckhardt
Chris Campbell
Arthur Cole
Heather Crawford
Barry Davids
Paul DeYoung
Alfredo Estrade
Paul Fallon
Joe Finck
Nathan Frank
Alexandra Gade
Umesh Garg
Sierra Garrett
Jacklyn Gates
Hans Geissel
Kenneth Gregorich
Paul Gueye
Magne Guttormsen
Christine Hampton
Marc Hausmann
Jerry Hinnefeld
Calem Hoffman
Hironori Iwasaki
Robert Janssens
Kate Jones
Zach Kohley
Toshiyuki Kubo
Anthony Kuchera
Sushil Kumar
Jonathan Kustina
Christoph Langer
Ann-Cecilie Larsen
Bill Lynch
Augusto Machiavelli
Wolfgang Mittig
Shea Mosby
Chiara Nociforo
Shumpei Noji
Hideaki Otsu
Mauricio Portillo
Lew Riley
Warren Rogers
Andrew Rogers
Brad Sherrill
Jenna Smith
Artemis Spyrou
Sharon Stephenson
Krystin Stiefel
Chris Sullivan
Oleg Tarasov
Michael Thoennessen
Aditya Wakhle
Helmut Weick
Dirk Weisshaar
Ingo Wiedenhoever
Scott Williams
Kathrin Wimmer
John Stuart Winfield
Martin Winkler
John Stuart Yurkon
Remco Zegers
Al Zeller

This whitepaper was edited by Alexandra Gade and Remco Zegers. Pre-conceptual design studies for the HRS and beam line were performed by Thomas Baumann and Marc Hausmann. Front cover art by Erin O'Donnell and Thomas Baumann.